Incorporation of Ru(II) Polypyridyl Complexes into Nanomaterials for Cancer Therapy and Diagnosis

Nancy Soliman, Gilles Gasser, Christophe M Thomas

Incorporation of Ru(II) Polypyridyl Complexes into Nanomaterials for Cancer Therapy and Diagnosis

Nancy Soliman,[a,b] Gilles Gasser,[b,*] and Christophe M. Thomas[a,*]

[a] Chimie ParisTech, PSL University, CNRS, Institut de Recherche de Chimie Paris, 75005 Paris, France. E-mail: christophe.thomas@chimie-paristech.fr; WWW: https://www.ircp.cnrs.fr/la-recherche/equipe-cocp/

[b] Chimie ParisTech, PSL University, CNRS, Institute of Chemistry for Life and Health Sciences, Laboratory for Inorganic Chemical Biology, 75005 Paris, France. E-mail: gilles.gasser@chimieparistech.psl.eu; WWW: www.gassergroup.com

ORCID-ID:

Nancy Soliman: 0000-0002-3031-8584

Gilles Gasser: 0000-0002-4244-5097

Christophe M. Thomas: 0000-0001-8014-4255

KEYWORDS: Anticancer; Medicinal Inorganic Chemistry; Metals in Medicine; Nanomaterials, Nanomedicine.

Abbreviations

AFM = atomic force microscopy, AuNPs = gold nanoparticles, AgNPs = silver nanoparticles, BCPs = block copolymers, CNAs = cross-linked nanoassemblies, CNTs = carbon nanotubes, DLS = dynamic light scattering, EPR = enhanced permeability and retention, FDA = Food and Drug Administration, HSA = human serum albumin, M_n = number average molecular weight, MOFs = metal-organic frameworks, MSNs = mesoporous silica nanoparticles, MWCNTs = multi-walled carbon nanotubes, PACT = photoactivated chemotherapy, PEG = poly(ethylene glycol), PDI = polydispersity index, PDT = photodynamic therapy, PLA = polylactide, PLGA = poly(lactide-*co*-glycolide), PS = photosensitizer, PTT = photothermal therapy, RAFT = radical addition-fragmentation transfer, rGO = reduced graphene oxide, ROS = reactive oxygen species, SEC = size exclusion chromatography, SEM = scanning electron microscopy, SeNPs = selenium nanoparticles, SiNPs = porous silicon nanoparticles, SQ =squalene, SWCNTs = single-walled carbon nanotubes, TEM = transmission electron microscopy UCNPs = upconversion nanoparticles, 2P = two-photon, 1P = one-photon

Abstract

Ru(II) polypyridyl complexes are compounds of great interest in cancer therapy, due to their unique photophysical, photochemical and biological properties. For effective treatment, they must be able to penetrate tumor cells effectively and selectively. The development of nanoscale carriers capable of delivering Ru(II) polypyridyl complexes has the potential to passively or selectively enhance their cellular uptake in tumor cells. Many different strategies have been explored to incorporate Ru(II) polypyridyl complexes into a variety of nano-sized constructs, ranging from organic to inorganic materials. This review serves to highlight recent developments in nanomaterials loaded with Ru(II) polypyridyl complexes. Their rational design, preparation and physicochemical properties are described, and their potential applications in cancer therapy are eventually discussed.

1. Introduction

Cancer is a disease caused by the uncontrollable growth of abnormal cells. It is one of the leading causes of death in the world, accounting for around 10 million deaths each year.[1] This alarming

data brings up the necessity to develop efficient methods for the diagnosis and treatment of cancer. In this regard, metal-based drugs have been highly investigated for different medicinal applications against various cancer-related issues, especially since the discovery of cisplatin in the late 1960s. Among them, Ru(II) complexes and in particular Ru(II) polypyridyl complexes have drawn increased attention in recent years due to their unique and appealing photophysical and photochemical properties, which can be tuned by varying the nature and the numbers of the polypyridyl ligands around the Ru(II) metal center.[2] They absorb light and emit wavelength within the red and the near infrared (NIR) spectral regions and possess large Stokes shift, long luminescence lifetime, and potential two-photon (2P) absorption properties. These characteristics have made them highly desirable across numerous research fields such as catalysis,[3] solar energy,[4] sensors[5] and now across the biomedical field either in diagnostics as cellular imaging tools, luminescent probes of DNA structures or in therapy as new classes of anticancer drugs for chemotherapy and photosensitizers (PSs) for photodynamic therapy (PDT) or photoactivated chemotherapy (PACT).[6-11] Worthy of note, a Ru(II) polypyridyl compound (TLD1433) has recently entered phase II clinical trials in Canada for the treatment of non-muscle invasive bladder cancer as a PS for PDT.[12] However, these complexes still suffer from some drawbacks such as poor water solubility, lack of targeting capability, nonspecific distribution, systemic toxicity and hence, low therapeutic index hampering their translation into the clinic. One strategy to address those medical challenges is to use nanomedicine. Nanomedicine is the application of sub-micron particles (*i.e.*, nanoparticles) in the field of medicine. The materials used for the synthesis and/or formulation of nanoparticles are extremely diverse, ranging from organic to inorganic molecules (Figure 1).[13] The unique features of nanoparticles including small size, high surface area, surface chemistry, water solubility and multi-functionality make them highly interesting for drug delivery purposes.[14,15] Owing to their size, nanoparticles can passively accumulate to solid tumors while sparing healthy cells thanks to the enhanced permeation and retention (EPR) effect.[16] The EPR effect exploits the abnormalities of tumor vasculature, namely hypervascularity, atypical vascular architecture, leaky vasculature, and lack of lymphatic drainage. This results in the efficient extravasation of nanoparticles from the tumor vasculature and their retention in the tumor interstitium. Therefore, drug incorporation into nanoparticles provides significant improvements in pharmacokinetics, solubility, toxicity and biodistribution when compared

to freely administered molecules, reducing adverse side effects observed with conventional medicine. However, to take full advantage of the EPR effect, nanoparticles must remain in circulation long enough for tumor accumulation. PEGylation, which refers to modification with poly(ethylene glycol) (PEG) chains or PEG copolymers (*e.g.*, Jeffamine), is the most common strategy for imparting stealth properties to nanoparticles.[17] The presence of PEG enables steric stabilization preventing particle interactions, protein adsorption, phagocytic uptake by macrophages, and interactions with immune cells. Nanoparticles can be further modified with ligands that have binding affinity for receptors overexpressed in tumor cells to allow active targeting.[18] Although it is widely held to improve delivery of nanodrugs to tumors, the EPR effect remains controversial and subject to debate.[19] Among materials available for constructing nanomedicines, liposomes and polymers are the most widely used and the promising ones.[20] The early discoveries in polymer encapsulation of metal complexes for biological and medicinal applications have been extensively and remarkably covered and will not be duplicated herein.[21,22] The present review is concerned with recent selected papers that have described methodologies and strategies that allow incorporation of Ru(II) polypyridyl complexes into a variety of nanomaterials for cancer-related biomedical applications.

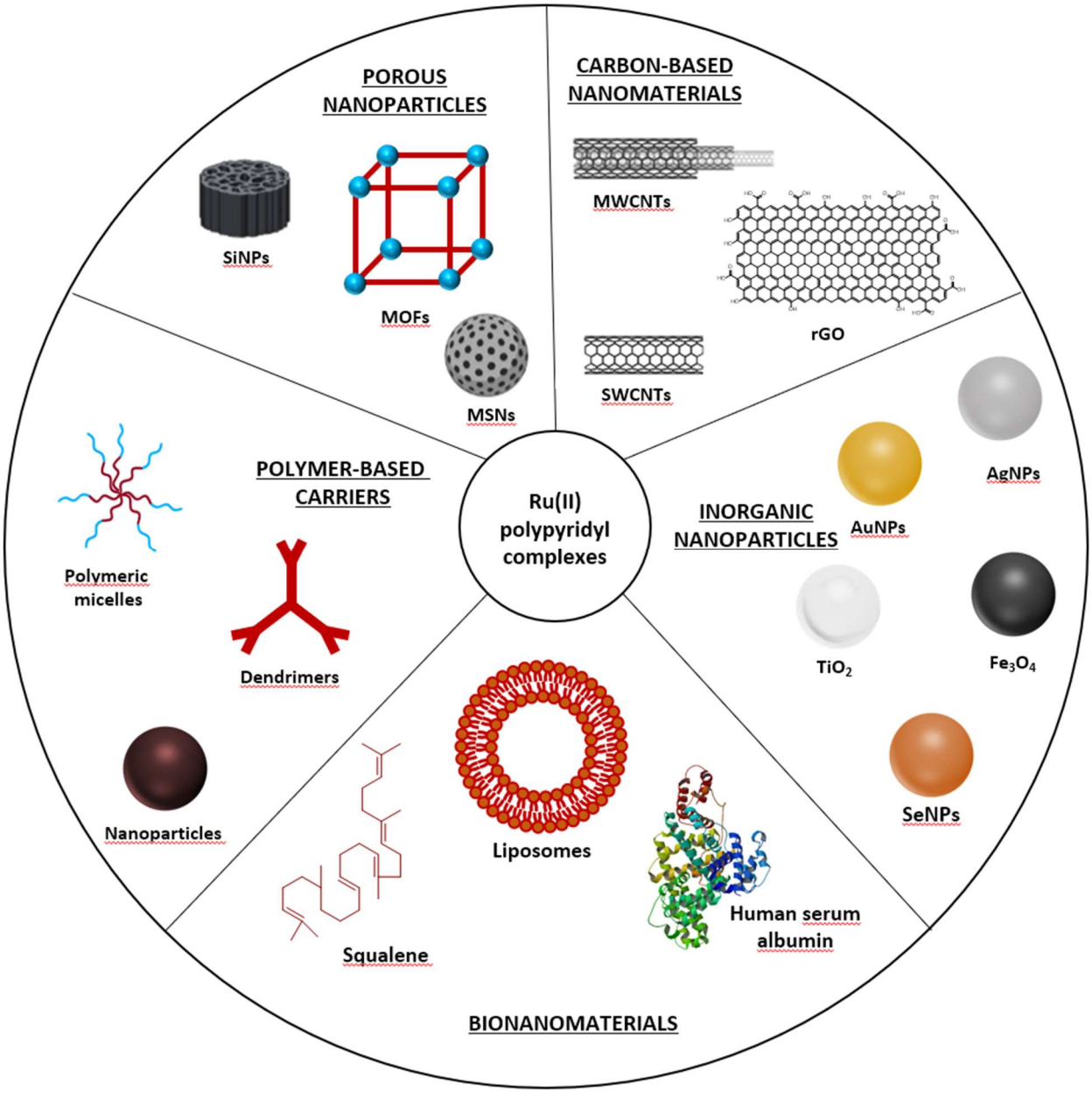

Figure 1. Schematic representation of the nanosized constructs reported for the incorporation of Ru(II) polypyridyl complexes

2. Organic nanoparticles

2.1. Polymeric nanocarriers

Polymer-based nanocarriers have been adopted as the preferred system for drug delivery because of their ease of synthesis, their great diversity of composition, architecture and functionalization and their ability (for most of them) to degrade in physiological media. Thanks to the great diversity of polymer architectures, a wide range of polymeric nanomaterials - comprising micelles, nanoparticles, nanogels, vesicles and dendrimers – is accessible, which make them an important class of drug

delivery systems. Polymeric micelles are obtained by the self-assembly of amphiphilic polymers where the hydrophobic core of the micelles creates a microenvironment for the encapsulation of therapeutic compounds and the hydrophilic shell provides a stabilizing interface between the hydrophobic core and the aqueous medium. Nanogels are made of three-dimensional cross-linked networks of hydrophilic polymers while dendrimers are highly branched macromolecules that form a tree-like structure. As to polymer nanoparticles, they are solid particles composed of macromolecular polymers regardless of their structure.

Drugs can be encapsulated into polymer matrix using two different strategies: (i) physical encapsulation relying on non-covalent interactions between drugs and polymer matrix and (ii) covalent encapsulation where the drug is covalently conjugated to the polymer. In most cases, drugs are physically encapsulated into the polymer matrix. However, this type of encapsulation suffers from important limitations such as (i) “burst release”, which consists in the abrupt release of a large amount of drug post administration; (ii) the difficulty to encapsulate drugs that are poorly miscible to the polymer matrix and (iii) poor drug loading (less than 10 %), thus requiring a high concentration of drug delivery systems to obtain a therapeutic effect. To overcome these drawbacks, a covalent encapsulation has been considered. Three synthetic strategies can be used to obtain drug-polymer conjugates: (i) the drug can be conjugated to a pre-synthesized polymer or (ii) to a monomer prior to polymerization, or (iii) the drug can, after appropriate functionalization, serve as a polymerization initiator.[23] When drugs are transition metal complexes, drug-polymer conjugates can also be prepared by chelation of a polymeric macroligand to the metal precursor. Either way, polymeric nanosystems can be formulated using the following techniques: (i) emulsification and solvent evaporation/extraction, (ii) nanoprecipitation (also known as solvent-displacement method),[24] (iii) supercritical anti-solvent method, (iv) dialysis, and (v) salting-out method.[25] Among these techniques, emulsification, solvent evaporation/extraction, and the nanoprecipitation methods are by far the most widely employed.

2.1.1. Physical encapsulation

Aliphatic polyesters such as FDA-approved polylactide (PLA) and poly(D,L-lactide-*co*-glycolide) (PLGA) are the most used biodegradable and biocompatible polymers in drug delivery systems. The

physical properties, and degradation of these polymers, which proceeds through the hydrolysis cleavage of ester bonds, can be tuned by varying the molecular weight, the stereochemistry, and the copolymer composition. The degradation of PLA and PLGA affords acidic products, namely lactic acid and glycolic acid, which are non-toxic and can be metabolized to give CO_2 and H_2O as benign by-products. [26]

Lemercier and co-workers reported the encapsulation of two 5-substituted-1,10-phenanthroline-based Ru(II) 2P-PDT PSs, **Ru1** and **Ru2** (Figure 2) in PLGA nanoparticles by nanoprecipitation in the presence of Poloxamer 188 (P188), from a commercially available acid terminated PLGA with a 50:50 D,L-lactide to glycolide ratio and a number average molecular weight M_n of 24 000 – 38 000 $g{\cdot}mol^{-1}$.[27] A drug loading of around 1 % could be achieved. As confirmed by dynamic light scattering (DLS) and atomic force microscopy (AFM), the authors obtained spherical 100 nm and narrowly dispersed nanoparticles with a polydispersity index (PDI) lower than 0.15. These nanoparticles were much less toxic in C6 glioma cells than the related free Ru(II) polypyridyl complexes after irradiation with a white light source. The release of Ru payloads was accelerated after irradiation: 50 % of Ru was released after two days as opposed to 10 % after six days without irradiation.

Chen and co-workers reported the encapsulation of $[Ru(phen)_2$-*p*-MOPIP$](PF_6)_2{\cdot}2H_2O$ (**Ru3**, *p*-MOPIP = 2-(4-methoxyphenyl)imidazo[4,5-f][1,10]phenanthroline, phen = 1,10-phenanthroline, Figure 2), a potential anticancer agent,[28] in PLGA nanoparticles (**PLGA@Ru**) using the nanoprecipitation technique from a commercially available PLGA with a 75:25 ratio of D,L-lactide to glycolide and a M_n = 50 000 $g{\cdot}mol^{-1}$.[29] The resulting 130 nm nanoparticles were then coated with a polyethylenimine (M_n = 10 000 $g{\cdot}mol^{-1}$), previously functionalized with biotin and poly(ethylene glycol) (PEG, M_n = 5 000 $g{\cdot}mol^{-1}$), **Bio-PEI-mPEG**. They obtained 150 nm spherical **Bio-PLGA@Ru** nanoparticles with active targeting ability towards cells overexpressing biotin receptors. Cytotoxicity of **Bio-PLGA@Ru** was evaluated in different cancer cell lines (*i.e.*, HepG2 human hepatocellular carcinoma cells, A375 human malignant melanoma cells, HeLa, Siha and Caski human cervical carcinoma cells) and in a non-cancerous cell line (*i.e.*, NIH3T3 mouse fibroblast cells) and compared to the uncoated **PLGA@Ru** and the free Ru complex, **Ru3**. **Bio-PLGA@Ru** nanoparticles enhanced the accumulation of **Ru3** in cancer cells by the lipid raft-mediated endocytosis pathway causing a

cytotoxicity against HepG2 cells 3-4 folds higher than those of **Ru3** and **PLGA@Ru**. This might be explained by a higher intracellular ROS levels, hence a higher level of DNA damage. Biodistribution in HepG2 xenograft nude mice revealed that **Bio-PLGA@Ru** was mainly accumulated in the liver and tumor regions while **Ru3** was distributed around the whole mice body, showing how the nanoparticle formulation could improve the biodistribution of **Ru3** in the body.

Glazer and co-workers focused on improving the efficacy of Ru complexes for PDT by employing cross-linked nanoassemblies (CNAs) as a nanogel delivery platform.[30] They used polymeric CNAs obtained from poly(ethylene glycol)-*block*-poly(L-aspartate) copolymers (PEG-*b*-PASP, M_n = 6 100 g·mol^{-1} as determined by ^{1}H NMR spectroscopy), two Ru-based photoactivatable prodrugs with varying levels of hydrophobicity, namely $[Ru(bpy)_2(dmbpy)]Cl_2$ (**Ru4**, bpy = 2,2′-bipyridine, dmbpy = 6,6′-dimethyl-2,2′-bipyridine) and $[Ru(dmbpy)_2(dip)]Cl_2$ (**Ru5**), as well as one photostable $[Ru(dip)_3]Cl_2$ (**Ru6**, dip = 4,7-diphenyl-1,10-phenanthroline, Figure 2). The Ru complexes were physically entrapped in PEG-*b*-PASP CNAs (M_n = 340 000 g·mol^{-1}) *via* the attractive ionic interactions between positively charged complexes and negatively charged aspartate (ASP) groups allowing drug loading up to 20 %. The CNAs, before and after Ru loading, were defined as relatively monodisperse with an average diameter of *ca.* 20 nm and a PDI of *ca*. 0.25. The release rate and the amount of Ru(II) complex released from PEG-*b*-PASP CNAs were found to depend on complex hydrophobicity and solution ionic strength. However, the cytotoxicity of Ru-loaded CNAs in A549 human lung adenocarcinoma, before and after irradiation (λ > 400 nm, 5 min), was similar to the one obtained with the parent Ru(II) complexes. **Ru4**, loaded or not in PEG-*b*-PASP CNAs, was not toxic in the dark with an EC_{50} > 300 μM, while photocytotoxicity was observed after irradiation with an EC_{50} of 8.3 ± 1.2 μM for the free Ru complex and 12.9 ± 1.1 μM when loaded in PEG-*b*-PASP CNAs. As to **Ru5** and **Ru6**, loaded or not, they were already toxic in the dark (EC_{50} = 9.7 ± 1.3 μM and EC_{50} = 0.6 ± 1.1 μM, respectively) and had EC_{50} values in the micromolar range after irradiation (EC_{50} = 3.9 ± 1.1 μM and EC_{50} = 0.1 ± 1.1 μM, respectively).

Gallei, Gasser and co-workers described the encapsulation of a Ru(II) polypyridyl PDT photosensitizer, $[Ru(bpy)_2$-dppz-7-hydroxymethyl$](PF_6)_2$ (**Ru7**, dppz = dipyrido[3,2-a:2',3'-c]phenazine, Figure 2) in stimuli-responsive block copolymers with poly(*N*,*N*-dimethylaminoethyl

methacrylate) (PDMAEMA) as the hydrophilic segment and either poly(methyl methacrylate) (PMMA) or a statistical copolymer PMMA-*co*-PDMAEMA as the hydrophobic segment.[31] These polymers showed a low critical solution temperature (LCST) behavior in water: micelles were formed below LCST and shrinkage of micelles occurred above LCST allowing the release of Ru payloads. This temperature could be tailored by varying ionic strength and the ratio of MMA to MAEMA. Not only the release of Ru(II) complex could be triggered by temperature, it could also be triggered by pH variation and ultra-sound. However, as the LCST was too low (*i.e.*, around room temperature), no biological tests were reported. Therefore, more research will need to be performed for the synthesis of these copolymers with LCST around 37 – 43 °C to allow the controlled release of the Ru complex in pharmaceutically relevant temperature using hyperthermia for example.[32]

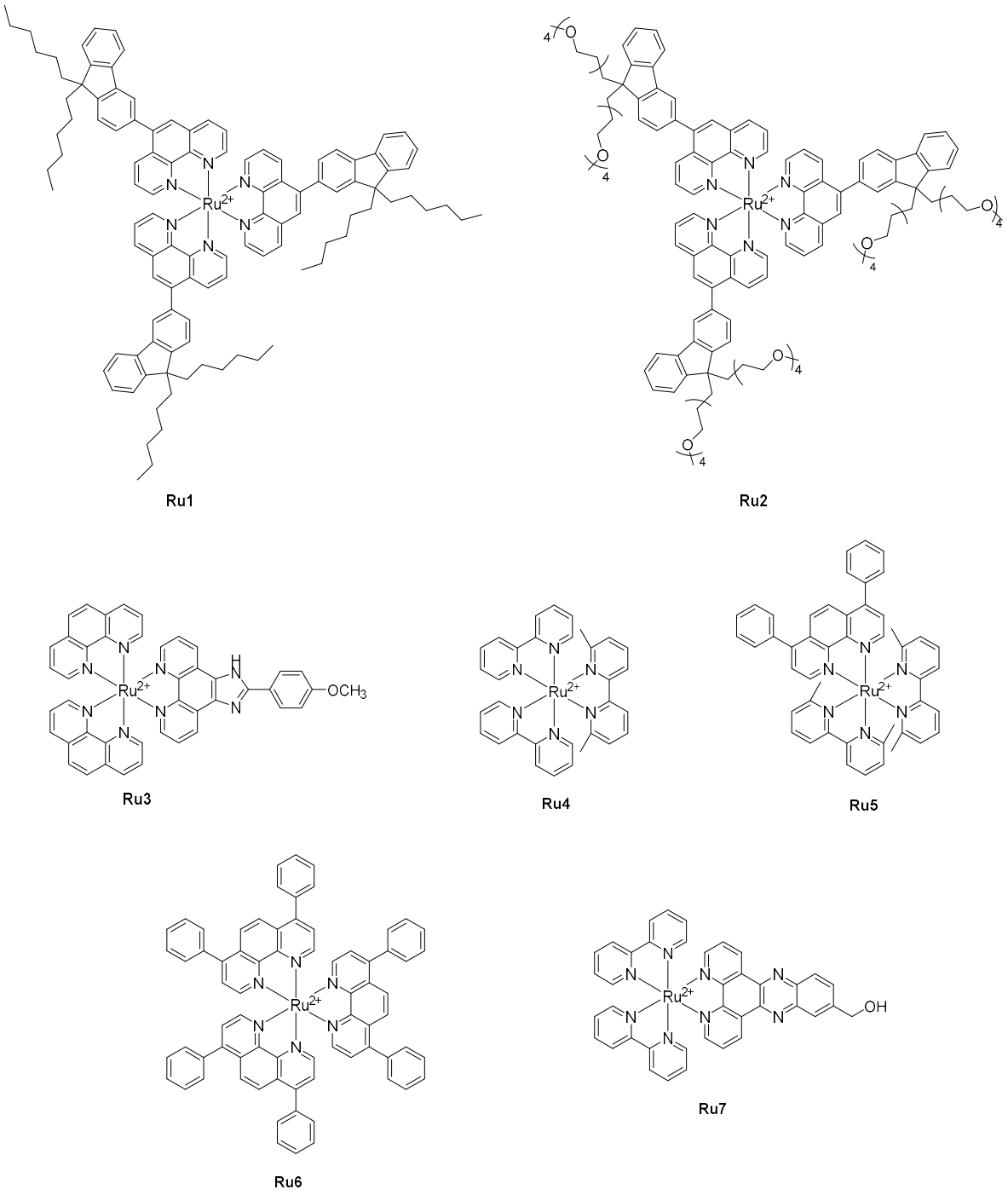

Figure 2. Chemical structures of **Ru1-Ru7**.

2.1.2. Covalent encapsulation

Covalent encapsulation is the formulation of polymer-drug conjugates into nano-sized constructs. The concept of polymer-drug conjugates, in which the drug is covalently linked to a hydrophilic polymer, was inspired by the prodrug approach and first introduced in 1975 by Ringsdorf.[33] Depending on where the Ru center is conjugated to the polymer (*e.g.*, the backbone, a lateral pendant group, the center of a star polymer), different synthetic strategies have been described.[34]

Ranucci, Maggioni and co-workers investigated the use of linear polyamidoamine (PAMAM) bearing pendant phenanthroline groups that could coordinate to $Ru(phen)_2(OTf)_2$ (**Ru8**, OTf = triflate anion, $CF_3SO_3^-$) for optical imaging and PDT applications. PAMAM copolymers were obtained by Michael polyaddition of 4-(4′-aminobutyl)-1,10-phenanthroline (BAP) with piperazine derivatives and bisacrylamide derivatives, followed by complexation with **Ru8**, which resulted in $[Ru(phen)_3]^{2+}$ lateral pendant groups linked to the PAMAM chain *via* butyl segments (Figure 3a). First, they reported the synthesis of an amphoteric PAMAM copolymer, namely PhenISA**,** with a M_n value of 46 800 $g{\cdot}mol^{-1}$, M_w/M_n of 1.78 and 6 % of phenanthroline-containing repeating unit, which could coordinate to **Ru8**.[35] The resulting polymer **Ru8-PhenISA** could self-assemble into nanoparticles with a diameter of *ca.* 20 nm that were able to internalize in HEK-293 cells *via* an endocytic pathway while displaying no cytotoxicity up to 50 µM, suggesting that this system could be used for imaging. They then decided to vary the structure of PAMAM by synthesizing **Ru8-PhenAN** with a M_n value of 34 600, M_w/M_n of 1.38 and 2 % of Ru-containing repeating units that could self-assemble into *ca.* 10 nm nanoparticles.[36] The PDT efficiency of **Ru8-PhenAN** was evaluated in HeLa cells and compared to that of **Ru8-PhenISA** and $[Ru(phen)_2(BAP)](OTf)_2$ (**Ru9**), a complex used as a model of the photoactive units. **Ru8-PhenAN** was found to be more cytotoxic than **Ru8-PhenISA** and **Ru9** in HeLa cells with an EC_{50} of 0.7 µM as opposed to 9 µM for the free complex upon visible light irradiation (40 min, 23.7 $mW{\cdot}cm^{-2}$). The reason is that **Ru8-PhenAN** accumulated preferentially in the nucleus unlike the free complex, which was found in the cytosol.

Wu and colleagues reported the synthesis of three well-defined amphiphilic Ru-containing block copolymers (BCPs) **P1**, **P2** and **P3** with varying molecular weights (M_n = 11.2, 15.7 and 16.9 $kg{\cdot}mol^{-1}$) and high Ru loading (%Ru = 41, 55 and 51 wt%) that could self-assemble into different sub-150 nm nanostructures including micelles, hollow spheres and large compound micelles (Figure 3b).[37] $[Ru(tpy)(biq)(H_2O)](PF_6)_2$ (**Ru10**, tpy = 2,2′:6′,2″-terpyridine and biq = 2,2′-biquinoline) was coordinated to a preformed polymer, poly(ethylene glycol)-*block*-poly(6-(4-cyanophenoxy) hexyl methacrylate) (PEG-*b*-PCPH), which was synthesized by reversible-addition fragmentation chain transfer polymerization (RAFT) polymerization of a methacrylate monomer, 6-(4-cyanophenoxy) hexyl methacrylate (CPH), using a PEG-based macro-RAFT agent. **P1**, in comparison with **P2** and

P3, showed a higher anticancer effect after light irradiation (656 nm, 30 mW cm^{-2}, 30 min) in HeLa cells attributed to a higher cellular uptake (hence, higher Ru intracellular concentration), the light-triggered release of **Ru10** – an anticancer therapeutic agent, IC_{50} = 3.5 $\mu g \cdot mL^{-1}$ in HeLa cells - and the generation of intracellular $^1O_2$.

This strategy is suitable for treatment of hypoxic tumor as it does not uniquely rely on the generation of $^1O_2$. Therefore, they used the same approach with a slightly different Ru complex $[Ru(CHLtpy)(biq)(H_2O)](PF_6)_2$ (**Ru11**), where the commercially available anticancer drug chlorambucil (CHL) was conjugated *via* an ester bond, for phototherapy against hypoxic tumors *in vitro* and *in vivo* (Figure 3b).[38] As explained above, **Ru11** was coordinated to a preformed block copolymer PEG-*b*-PCPH to give **P4** with a M_n value of 20 300 $g \cdot mol^{-1}$ and a Ru loading of *ca.* 45 wt% that could self-assemble into micelle-like nanoparticles with a diameter of *ca.* 15 nm as determined by TEM. The micelles showed negligible toxicity in the dark in HeLa cells under normoxic and hypoxic conditions. However, upon light irradiation (656 nm, 60 $J \cdot cm^{-2}$), they were found to be toxic in both conditions with an EC_{50} of 25 $\mu g \cdot mL^{-1}$ attributed to the release of the aqua adduct **Ru11**. The phototoxicity was O_2-independent.

The same authors later investigated the potential use of a Ru-containing ABA-type triblock copolymer (**PolyRu**) for combined photodynamic therapy and photochemotherapy (Figure 3c).[39] **PolyRu** was prepared through a multi-step synthesis: the polyol-containing Ru complex $[Ru(Biq)_2(Hob)_2][PF_6]_2$ (**Ru12**, Biq = 2,2′-biquinoline, Hob = 4-[(6- hydroxyhexyl)oxy]benzonitrile) was synthesized to react with 2,4-diisocyanato-1-methylbenzene *via* polycondensation to form Ru-containing polyurethanes before being functionalized by poly(ethylene glycol) methyl ether resulting in the formation of monodisperse **PolyRu** of M_n = 22 000 $g \cdot mol^{-1}$ as determined by ^1H NMR spectroscopy, and further confirmed by size exclusion chromatography (SEC), $M_{n,SEC}$ = 15 kg mol^{-1}, $M_{w,SEC}/M_{n,SEC}$ = 1.22). **PolyRu** could self-assemble, using a nanoprecipitation technique, into spherical 180 nm stealth nanoparticles as confirmed by TEM and scanning electronic microscopy (SEM). The biological activity of **PolyRu** nanoparticles was evaluated *in vitro* in HeLa, PC3 and HepG2 and *in vivo* in HeLa tumor bearing mice. They showed that **PolyRu** could accumulate in tumor sites after 12 h and inhibit tumor growth after irradiation at 656 nm (50 $mW \cdot cm^{-2}$, 30 min), a

wavelength in the therapeutic window (650 – 800 nm), ideal for the treatment of deep-seated or large tumors. This high anticancer effect was attributed to the light-triggered release of $[Ru(Biq)_2(H_2O)_2](PF_6)_2$ (**Ru13**), a potential anticancer agent, which was reported to inhibit malignant tumor growth with a IC_{50} of 25 $\mu g \cdot mL^{-1}$ in the dark and 2.5 $\mu g \cdot mL^{-1}$ after irradiation due to the generation of $^1O_2$.

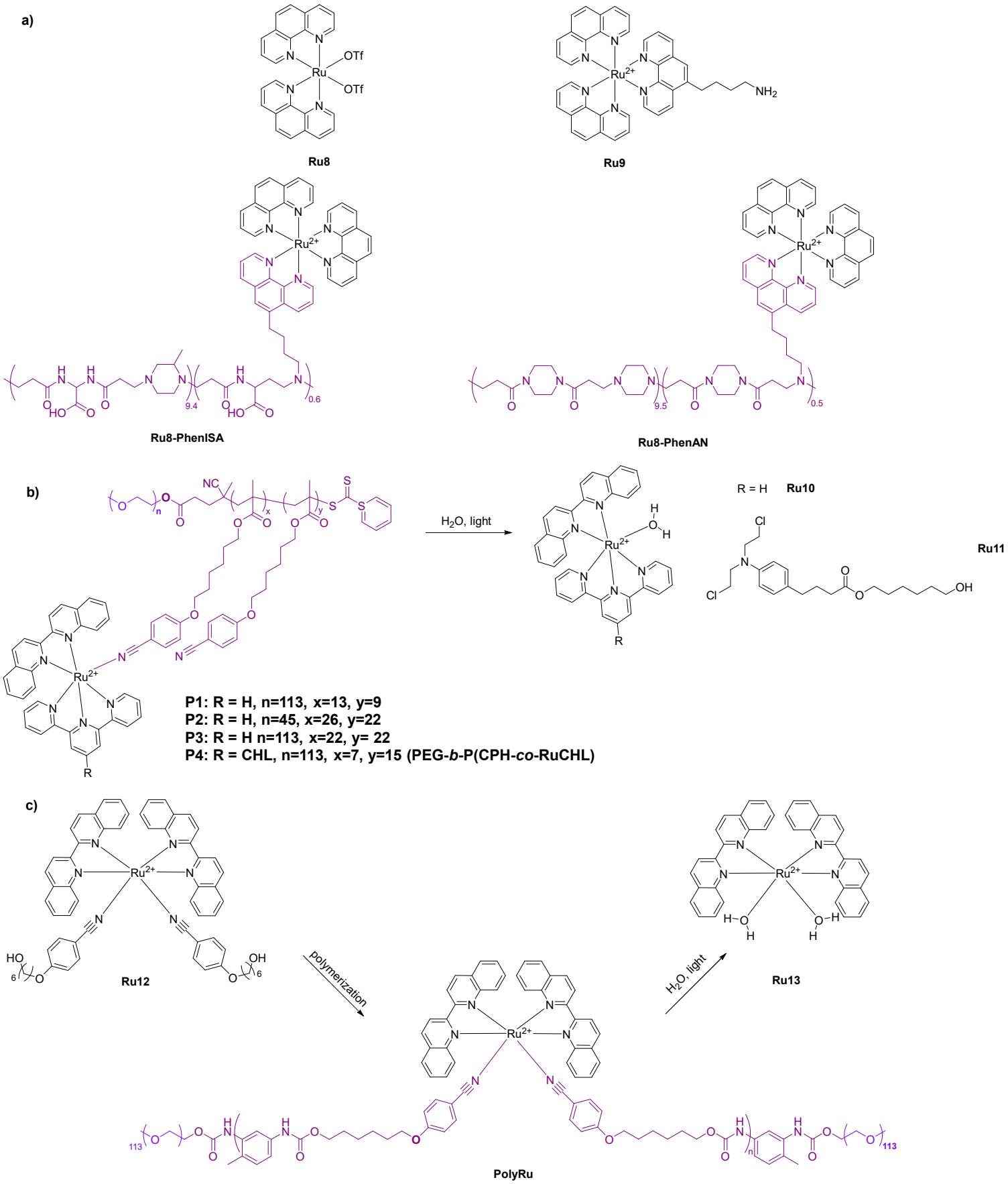

Figure 3. a) Structures of **Ru8** and the three $[Ru(phen)_3]^{2+}$ derivatives: **Ru9, Ru8-PhenAN** and **Ru8-PhenISA**. b) Chemical structures of PEG-*b*-PCPH of different chain lengths coordinated with **Ru10 or Ru11** to give **P1 – P4.** c) Structure of **Ru12**, **PolyRu** and **Ru13.** Ru(II) polypyridyl complexes are represented in black, polymers in purple with the PEG chains in blue.

In most of the articles reported so far, the Ru(II) complex is coordinated to the pendant group of a water-soluble polymer. This strategy possesses one key drawback, which is the lack of control over functional groups. To overcome this, drug-initiated polymerization, first described by Kricheldorf, in which a polymer chain is grown from the drug itself, can be considered to eliminate any possible heterogeneities.[40,41] Recently, we reported the one-pot synthesis of ruthenium-containing PLA by ruthenium-initiated ring opening polymerization of lactide from a non-cell penetrating PDT PS, namely [Ru(bipy)$_2$-dppz-7-hydroxymethyl](PF$_6$)$_2$ (**Ru7**).[42] These polymers **Ru7-PLA**, shown in Figure 4a, could further be formulated into size tunable nanoparticles from 100 to 300 nm by nanoprecipitation using poly(vinyl alcohol) as a stabilizer. All nanoparticles showed improved photophysical properties including luminescence, singlet oxygen generation, and enhanced cellular uptake in HeLa cells. Capitalizing on this, an improved photo-toxicity towards HeLa cells (λ = 480 nm, 3.21 J·cm^{-2}) with IC$_{50s}$ as low as 4.4 ± 0.8 μM after 48 h was determined while the free Ru complex showed no significant photocytotoxicity (IC$_{50}$ > 500 μM).

To obtain high drug loading, dendrimers can be used.[43] Velders and co-workers demonstrated that functionalization of PAMAM dendrimers with two Ru(II) polypyridyl complexes, **Ru14** and **Ru15** (Figure 4b), could afford 5 nm sized materials in water, as characterized by Diffusion-Ordered Spectroscopy (DOSY) NMR based on Pulse-Field Gradient Spin-Echo (PFGSE) measurements in D_2O, with improved fluorescent imaging properties.[44] The luminescence of these materials was 16-fold higher than that of the free Ru complexes, with no self-quenching observed. They mainly accumulated in the lysosomes of CT26 colon carcinoma cells, implying an internalization *via* passive endocytosis. The phototoxicity of these materials was evaluated qualitatively by confocal fluorescence microscopy, showing disruption of membrane integrity of CT26 cells treated with **Ru14-PAMAM** (carrying 32 positive charges) after irradiation at 405 nm for 30 min, while no change was observed with **Ru15-PAMAM** (carrying 32 negative charges). Because of their small size (*ca*. 5 nm), dendrimers are known to be rapidly cleared from the blood through the kidneys, which eliminate the need for biodegradability. Although promising, dendrimers are more expensive than other nanoparticles and require many repetitive synthetic steps, posing a challenge for large-scale production.

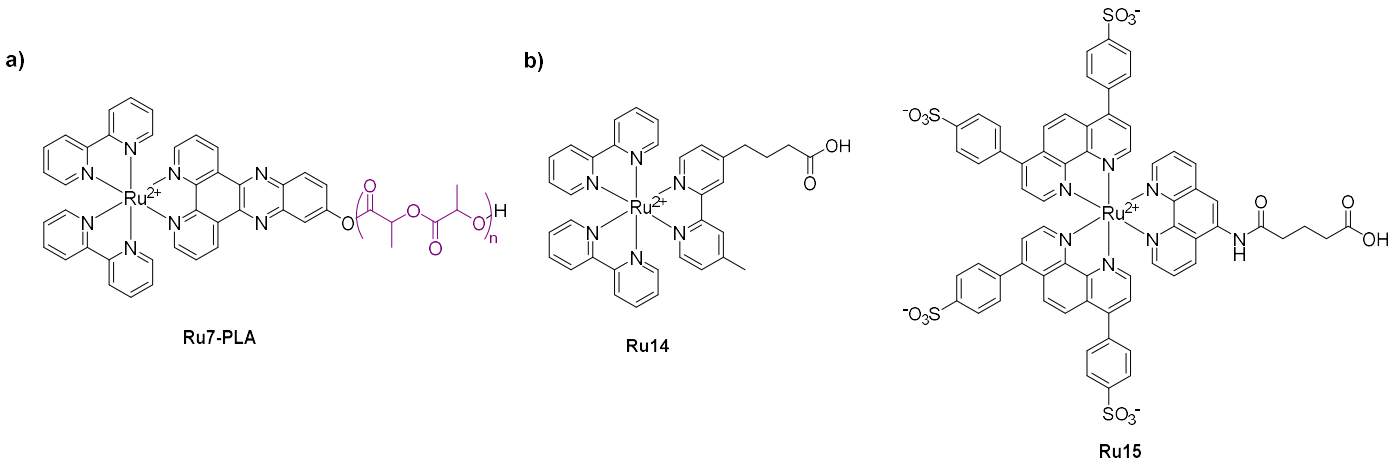

Figure 4. a) Structure of **Ru7-PLA**. b) Chemical structures of **Ru14** and **Ru15**. Ru(II) polypyridyl complexes are represented in black, polymers in purple.

2.2. Lipid-based nanocarriers

2.2.1. Liposomes

Liposomes are nano-sized to micro-sized vesicles consisting of an aqueous core surrounded by a phospholipid bilayer.[45] They were the first nanomedicine delivery system to make the transition from concept to clinical application making them an established technology platform with considerable clinical acceptance.

Shen, Mao and co-workers reported the encapsulation of the well-studied “light-switch” and active compound, $[Ru(phen)_2dppz](ClO_4)_2$ (**Ru16,** Figure 5a), in PEGylated sub-100 nm liposomes formed from dipalmitoylphosphatidylcholine (DDPC), PEG-modified phospholipid, 1,2-Distearoyl-*sn*-glycero-3-phosphoethanolamine-poly(ethylene glycol) (DSPE-PEG, M_n = 2 000 g mol^{-1}) and cholesterol with a Ru loading of 4 %.[46] The cytotoxicity of the resulting liposomes **LipoRu** was evaluated in MDA-MB-231 human breast cancer cells and compared to that of the free complex. **LipoRu** was much more cytotoxic than **Ru16** with an IC_{50} value lower than 4 µM while **Ru16** showed no toxicity up to 200 µM. This higher anticancer effect was attributed to a higher intracellular accumulation of **LipoRu**, which was 15-fold higher than that of the free Ru complex. For tumor specific imaging and therapy, a nanocarrier based on a 220 nm folate-conjugated liposome incorporating **Ru16** was proposed by Xie and co-workers.[47] The interaction between the nanocarrier and target HeLa cells overexpressing folate receptors (FARs) induced cell death after irradiation,

which was attributed to the effective light-triggered release of **Ru16** from the liposome carrier into the cytoplasm. No cytotoxicity was observed in the dark up to 100 µM.

Bonnet's research team examined the potential of ruthenium-decorated vesicles in the context of light-triggered release drug delivery.[48] By synthesizing a thioether-cholestanol hybrid ligand that could coordinate to Ru *via* its sulfur atom, they were able to decorate liposomes with Ru(II) polypyridyl complexes using either negatively charged lipids (1,2-dimyristoyl-*sn*-glycero-3-phospho-*rac*-(1-glycerol) sodium salt, DMPG) or neutral lipids (2-dimyristoyl-*sn*-glycero-3-phosphocholine, DMPC) to build up liposome membranes. They showed how it was possible to release $[Ru(trpy)(bpy)(H_2O)]^{2+}$ (**Ru18**) using light irradiation (Figure 5b). As NIR light is of great interest for treating deep-seated tumors, they focused on the preparation of liposomes capable of generating photons of blue light *in situ* by triplet-triplet annihilation (TTA) upconversion of either green or red light to trigger the photodissociation of $[Ru(tpy)(bpy)SRR']^{2+}$ (**Ru17**, SRR' = a monodentate thioether-cholestanol hybrid ligand) with a clinical grade PDT laser at 630 nm.[49] TTA principle relies on the conversion of low-energy protons into higher energy photons by a bimolecular mechanism, involving a photosensitizer and an annihilator molecule (*i.e.*, in this case, palladium tetraphenyltetrabenzoporphyrin and perylene, respectively). Two liposomal formulations were prepared separately and mixed together afterwards: one was made of DMPC, 4 mol% of DSPE-PEG, the photosensitizer and the annihilator molecule while the other was a Ru-functionalized liposomes made from the same lipids with a diameter ranging from 130 to 170 nm (Figure 5c). In 2015, the same authors combined all the components in one liposomal formulation with an average diameter of 130 – 180 nm and a PDI of 0.05 – 0.20, as determined by DLS (Figure 5d).[50] The clinical grade PDT laser at 630 nm could trigger the photodissociation of the Ru complex into its cytotoxic aqua species and in a faster way than the formulation described above. However, no biological evaluation was reported for both liposomal systems.

2.2.2. Lipid-drug conjugates: example of squalenoylation

Couvreur and his research team developed an original approach based on the use of squalene (SQ), a natural and biocompatible lipid involved in the cholesterol's biosynthesis, as a building block for the synthesis of SQ-drug conjugates.[51] The resulting SQ-drug conjugates could self-assemble in an

aqueous medium as nanoparticles, without the need for any surfactant and/or stabilizer. This concept called “squalenoylation” has been applied to commercially available anticancer agents, whether hydrophilic (*i.e.*, gemcitabine) or hydrophobic (*i.e.*, paclitaxel and cisplatin) and extended to a potential imaging agent, $[Ru(bpy)_2BIPPBI](PF_6)_2$ where BPPBI = 1-methyl-2-(4-methylpyridine-2-yl)-1H-benzoimidazole (**Ru19**). As SQ has no functional group, the SQ carbon core must be derivatized to react with drugs. For example, 1,1’,2-trisnorsqualenoic acid, a SQ derivative, can be obtained from squalene *via* a three-step synthesis involving squalene monobromohydrine and squalene-2-3-epoxide as intermediates. However, this process suffers from a very low yield of 5 %.[52] 1,1’,2-Trisnorsqualenoic acid can react with *N*-hydroxysuccinimide ester (NHS), SQ-NHS, for subsequent peptide coupling with a higher yield.

Gobetto and co-workers described the conjugation of the luminescent Ru(II) polypyridyl complex, $[Ru(bpy)_2BPPBI\text{-}hx](PF6)_2$ (**Ru20**, BPPBI = 6-[2-(4-methyl-pyridin-2-yl)-1H-benzoimidazol-1-yl]-hexylamine) to SQ-NHS *via* an amide bond (Figure 5e).[53] The resulting conjugate, **Ru20-SQ**, could self-assemble into narrowly dispersed 300 nm nanoparticles using a nanoprecipitation technique. **Ru20-SQ** was found to be non-toxic towards HT-29 colorectal (IC_{50} = 380 µM) and MCF-7 breast cancer cell lines (IC_{50} = 110 µM). While remaining non-toxic, this technique could improve the cellular uptake of **Ru19**, particularly in the nucleus, and diffuse into a more organized cell system: 3D multicellular tumor spheroids (MCTSs). This is ideal for cell imaging.

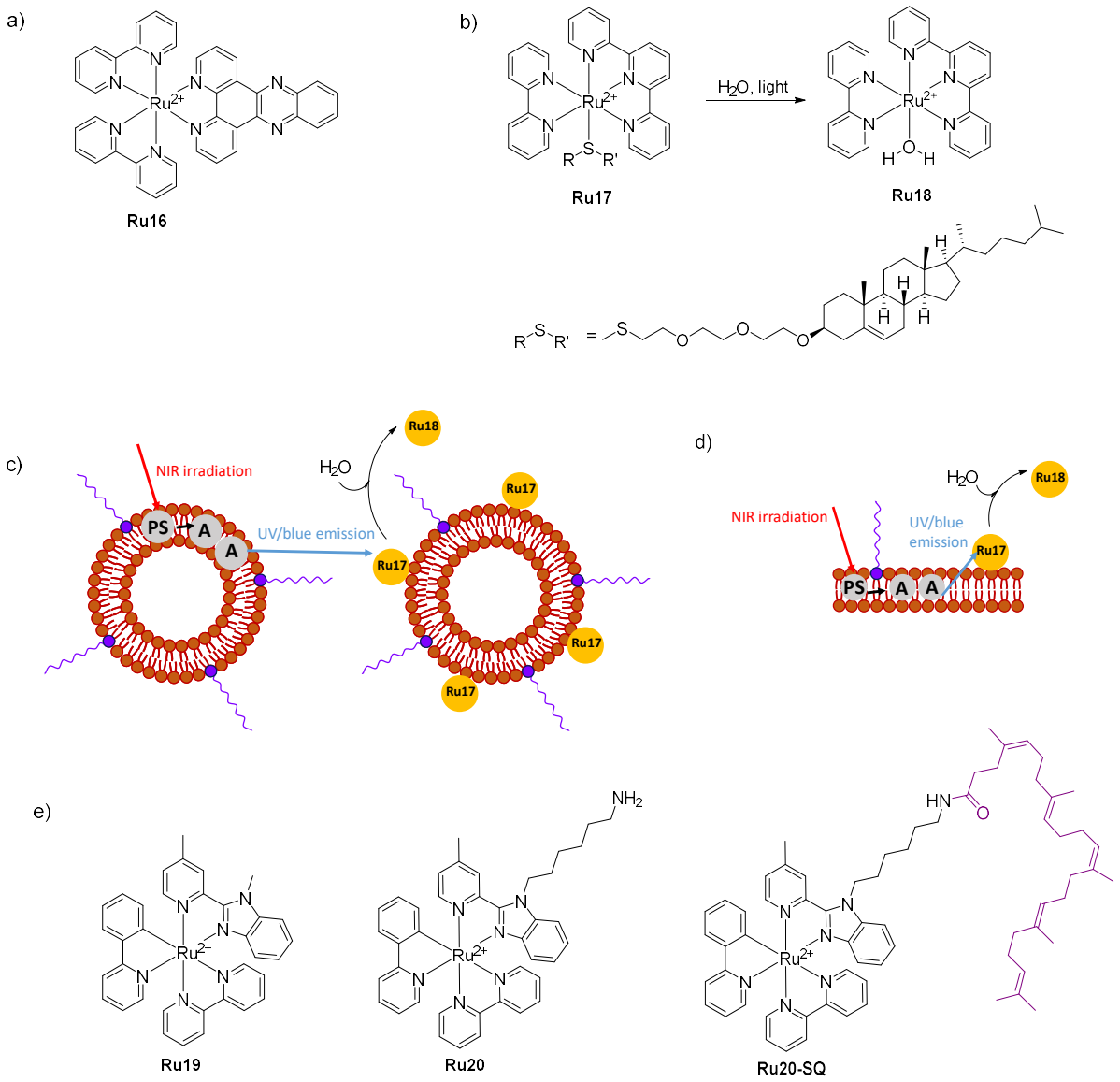

Figure 5. a) Chemical structure of $[Ru(phen)_2dppz]^{2+}$ (**Ru16**). b) Photoactivation of **Ru17** leading to the formation of the aqua adduct **Ru18**. c and d) Schematic representation of the liposomal formulations capable of generating blue light by TTA-UC. e) Chemical structures of **Ru19**, **Ru20** and **Ru20-SQ** with SQ derivative represented in purple.

2.3. Protein-drug conjugates

Protein-drug conjugates are proteins directly conjugated to drug molecules by a biodegradable bond that can self-assemble into nano-sized materials. Protein-drug conjugates are typically very small (< 50 nm), allowing the nanoparticle to have a long half-life *in vivo* and thus facilitating its delivery to the target tumor site. An inherent issue with protein-based nanoparticles is that the structural sensitivity of some drugs makes them difficult to bind to a protein base. As a result, certain drugs may not be suitable for this nanoparticle delivery system.

Weil and co-workers reported the conjugation of a PDT PS, $[Ru(bpy)_2(Hipa)_2]Cl_2$ where Hipa is 4-(1H-imidazo[4,5-f][1,10]phenanthroline-2-yl)-aniline (**Ru21**) to a PEGylated human serum albumin (HSA) bearing triphenylphosphonium (TPP) units for mitochondria targeting (Figure 6).[54] HSA, the most abundant protein in plasma, was functionalized with PEG (M_n = 2000 g mol^{-1}) to impart water solubility and reduce non-specific interactions, and with TPP units to give cHSA-PEO-TPP. Then, about 10 Ru complexes were conjugated to cHSA-PEO-TPP by reacting with the tyrosine side chains of HSA *via* a Mannich type reaction, resulting in the formation of a **cHSA-PEO-TPP-Ru21** nanomaterial with an average hydrodynamic radius of *ca*. 40 nm in water as well as in cell media. **cHSA-PEO-TPP-Ru21** exhibited significantly improved photophysical properties, enhanced $^1O_2$ quantum yields as well as excellent mitochondria specific colocalization in HeLa cells compared to the free Ru(II) complex. As a result, efficient phototoxicity (470 nm, 5 min, 20 mW cm^{-2}) of **cHSA-PEO-TPP-Ru21** was achieved at nanomolar concentrations in different cancerous cell lines: HeLa ($IC_{50light}$ = 34.9 ± 2 nM, PI = 250 as opposed to $IC_{50light}$ = 7.7 ± 1.3 µM, PI = 27 for the free Ru complex), CHO ($IC_{50light}$ = 135.2 ± 1 nM), MCF-7 ($IC_{50light}$ = 114.3 ± 1 nM), and A549 ($IC_{50light}$ = 119.1 ± 1 nM). In the absence of TPP units, the phototoxic effect of the drug was reduced by approximately 8-fold in HeLa cells ($IC_{50light}$ = 265 ± 1.2 nM). They also showed that **cHSA-PEO-TTP-Ru21** exhibited 2P luminescence with σ = 50 GM, attributed to the ruthenium complex. This feature was exploited by the Chao research team (see gold nanoparticles part).

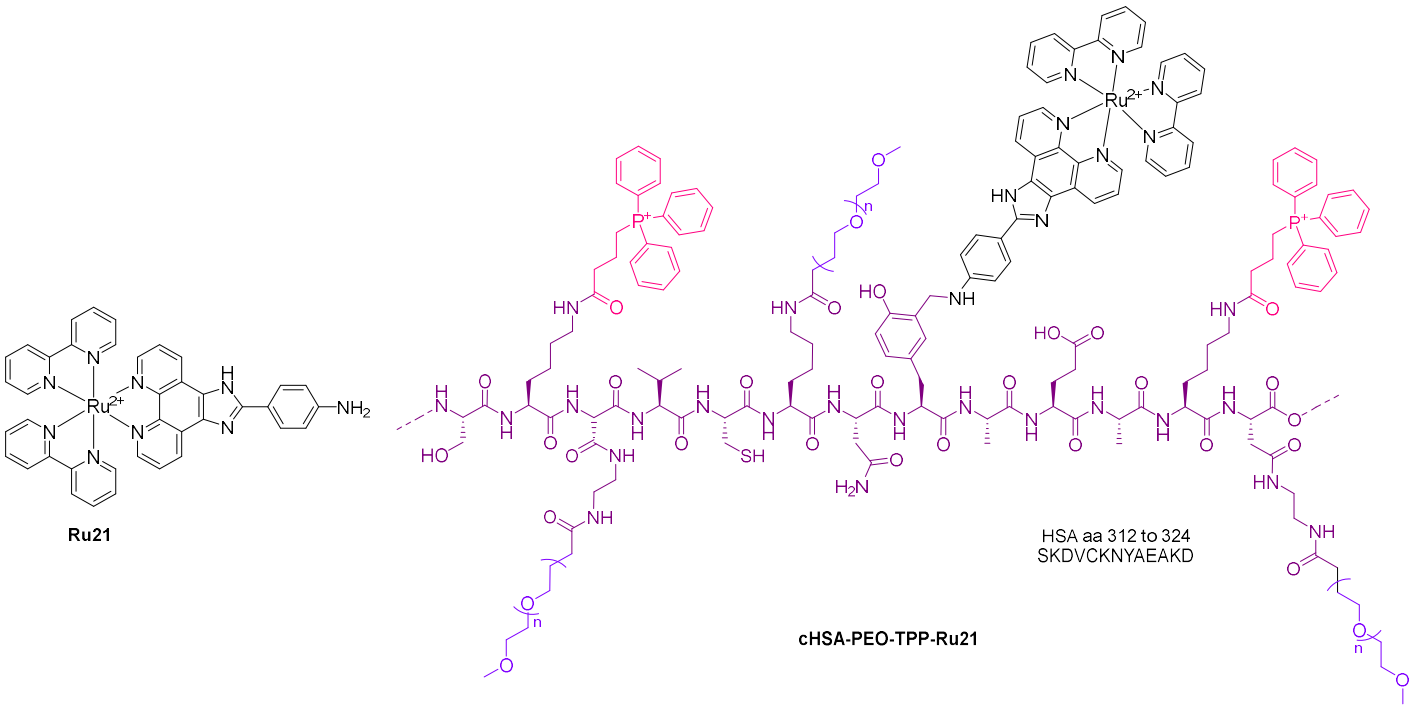

Figure 6. a) Chemical structure of $[Ru(bpy)_2Hipa]^{2+}$ (**Ru21**), b) Schematic illustration of a part of **cHSA-PEO-TPP-Ru21** showing how PEG (in blue), TPP (in pink) and **Ru21** (in black) are conjugated to HSA (in purple).

3. Inorganic nanoparticles

Inorganic nanoparticles are an important class of drug-delivery systems because of their rich variety, precision in size/shape control, excellent physicochemical properties, and multi-functionality. However, their inability to degrade has limited their scope of applications.

3.1. Carbon-based nanomaterials

Graphene consists of a layer with π-conjugated structure of six-atom rings forming a planar aromatic macromolecule.[55] This planar structure provides excellent ability to immobilize many substances, including drugs and fluorescent probes. Therefore, graphene has generated great interest in nanomedicine and biomedical applications, where suitably modified graphene can be used as a drug delivery platform for cancer treatment. Also, graphene is a basic building block for other graphitic materials with different geometries, such as carbon nanotubes (CNTs). Graphene-based nanomaterials have been shown to be able to destroy cancer cells by photothermal heating. This inherent feature makes them highly interesting for multi-modal therapy.

3.1.1. Reduced graphene oxide

Among graphene-based nanomaterials, reduced graphene oxide sheet (rGO) is one of the most effective photothermal therapy (PTT) agents that can absorb NIR light and induce a temperature increase in the local environment, causing irreversible cell damage. Mao and co-workers developed a nano-theranostic platform, in which a PDT PS and a phosphorescent PEG-modified Ru(II) complex, **Ru22** were loaded onto the PPT agent rGO surface *via* π-π and intermolecular hydrophobic interactions for the combination of PDT, PTT and imaging (Figure 7).[56] The resulting nanomaterials **rGO-Ru22**, with a thickness of 25 nm as characterized by AFM, showed a higher photothermal effect than naked rGO (ΔT = 33 °C as opposed to ΔT = 22 °C for rGO at 808 nm, 10 min, 1 $W{\cdot}cm^{-2}$) and enhanced cellular uptake in human lung cancer A549 cells (15.40 ± 0.69 ng 10^{-6} cells as opposed to 9.46 ± 0.43 ng 10^{-6} cells for **Ru22**). However, the ability of **rGO-Ru22** to produce $^1O_2$ upon irradiation at 450 nm was lower than that of **Ru22**, which could be due to the quenching effect caused by the photoinduced electron transfer between **Ru22** and rGO. Complete release of **Ru22** from **rGO-Ru22** after irradiation at 808 nm for 5 min (0.5 $W{\cdot}cm^{-2}$) could restore the ability of PS to produce $^1O_2$. By capitalizing on these, **rGO-Ru22** showed higher anticancer efficacy in a combined PTT−PDT treatment compared to PTT or PDT treatment alone. At 6.25 μM, cell viability for PTT treatment (808 nm, 0.5 $W{\cdot}cm^{-2}$, 5 min), PDT treatment (450 nm: 20 $mW{\cdot}cm^{-2}$, 2 min), and successive PTT−PDT treatment was 17.6 ± 3.6 %, 51.8 ± 1.0 % and 8.3 ± 0.5%, respectively, although no significant toxicity was observed in the dark. These results were further confirmed *in vivo* in mice bearing A549 tumors: combined PDT-PTT could significantly inhibit the growth of tumors.

3.1.2. Carbon nanotubes

Carbon nanotubes (CNTs) are well ordered tubular allotropes of carbon with a diameter in the nanometer range and a length reaching up to several centimeters.[57a] They can be single graphene sheet rolled up to form hollow tubes with walls one atom thick (single-walled carbon nanotubes, SWCNTs) or a multiple layer of graphene rolled simultaneously to form concentric tubes (multi-walled carbon nanotubes, MWCNTs). However, the apparent toxicity of CNTs has caused concerns for their use in drug delivery explaining its little use.[57b] To date, only one example for each CNTs type has been reported for the encapsulation of Ru(II) polypyridyl complexes. In addition to offering

potential drug delivery systems, CNTs have physical intrinsic properties including photothermal ones that could facilitate therapy and be used to develop innovative multi-modal therapies.

Chao and co-workers reported the loading of two photon-absorbing Ru(II)-based PDT PSs, **Ru23** and **Ru24**, onto commercially available SWCNTs of 0.7−1.3 nm diameter by π-π interactions after sonication in water.[58] The resulting nano-systems **Ru@SWCNTs**, stable up to three months in solution, were characterized with a length ranging from 20 nm to several micrometers by TEM imaging. The photothermal effect triggered the release of Ru(II) complexes, which produced $^1O_2$ upon two-photon laser irradiation (808 nm). **Ru@SWCNTs** showed a higher cancer killing effect than that of the free Ru(II) complexes and pristine SWCNTs upon 2P 808 nm light irradiation (0.25 W cm^{-2}, 5 min) in HeLa monolayer cancer cells as well as in 3D multicellular tumor spheroids (MCTSs) and *in vivo* on nude mice bearing a HeLa tumor model. Half of Ru complexes were released after 5 min of irradiation. They were found to localize in lysosomes, implying endocytosis as the mode of cellular uptake **Ru@SWCNTs.**

Chen and co-workers described the use of MWCNTs as a radiosensitive nanodrug delivery system for **Ru3** (Figure 2) in liver cells, including the multidrug resistant hepatocellular carcinoma R-HepG2, HepG2 and human hepatic L02 cell lines.[59] Approximately 9.8 % of **Ru3** could be loaded into Jeffamine-functionalized MWCNTs (M_n = 1 900 g·mol^{-1}) with an average diameter of 225 nm *via* π-π interactions. The resulting **Ru3@MWCNTs** nanoparticles were found to enhance the cellular uptake of **Ru3** in R-HepG2 cells *via* endocytosis and to have some cytotoxicity (IC_{50} = 40 ng·mL^{-1})**.** No significant toxicity (>80 % cell viability) was observed with unloaded MWCTs up to 160 ng·mL^{-1}. **Ru3@MWCNTs** showed significantly lower cytotoxicity towards healthy cells (*i.e.*, L02 cell lines) due to 1-2 fold lower cellular uptake. After being taken up by the cells, **Ru3@MWCNTs** were found in lysosomes, where **Ru3** could be released more rapidly due to the acidic nature of the lysosomes. Moreover, the sensitivity of R-HepG2 cells to ionizing radiation at a dose of 8 J·kg^{-1} was increased due to ROS overproduction: at 40 ng·mL^{-1}, cell viability went down to 20 % instead of 44.8 % without irradiation.

3.1.3. Carbon nanodots

Due to their intrinsic upconversion fluorescence, carbon nanodots (CDs) hold a great advantage in imaging and therapy that requires the use of NIR irradiation.

Mao, Tan and co-workers designed Ru complex modified CDs for lysosome-targeted 1P and 2P imaging and PDT.[60] **Ru25** was incorporated onto the surface of CDs using a typical EDC/NHS coupling reaction. Nanoparticles with a diameter of *ca.* 100 nm were obtained with a Ru loading of 4 %. The nanoparticles exhibited a higher 2P absorption cross-section than the free Ru complex at 810 nm (σ = 1118 GM as opposed to σ = 810 GM for **Ru25**) attributed to CDs. In addition, conjugation to CDs could improve the cellular uptake of **Ru25,** resulting in a higher inhibitory effect on cancer cell growth and an enhanced photodynamic efficiency in both 2D A549 cell ($IC_{50,light}$ = 3.0 ± 0.2 μM, PI > 20 after irradiation with visible light for 5 min, 20 mW cm^{-2}) and 3D multicellular tumor spheroid models ($IC_{50,light}$ = 2.2 ± 0.2 μM, PI > 45.4 after 810 nm irradiation for 20 min). These nanoparticles were also suitable for 2P imaging as shown on zebrafish.

Qu and co-workers developed a biocompatible imaging nanoplatform to monitor the oxygen level in HeLa cells.[61] An oxygen sensitive Ru(II) polypyridyl complex **Ru26** was conjugated to CDs using a EDC/NHS coupling reaction. The modified CDs were then PEGylated to form stealth and stable spherical nanoparticles in aqueous solution with diameters of 37 ± 5 nm, which could serve as an oxygen sensitive probe upon 720 nm NIR irradiation. While remaining non-toxic up to 0.4 μmol mL^{-1}, the PEGylated CDs could be imaged in HeLa cells after being excited at 720 nm, confirming the upconverted imaging capacity of these nanoparticles. The luminescence intensity was higher in hypoxic environment than in normoxic environment. *In vivo* imaging in mice bearing HeLa tumors showed that these nanoparticles could accumulate preferentially in the tumor rather than in other organs.

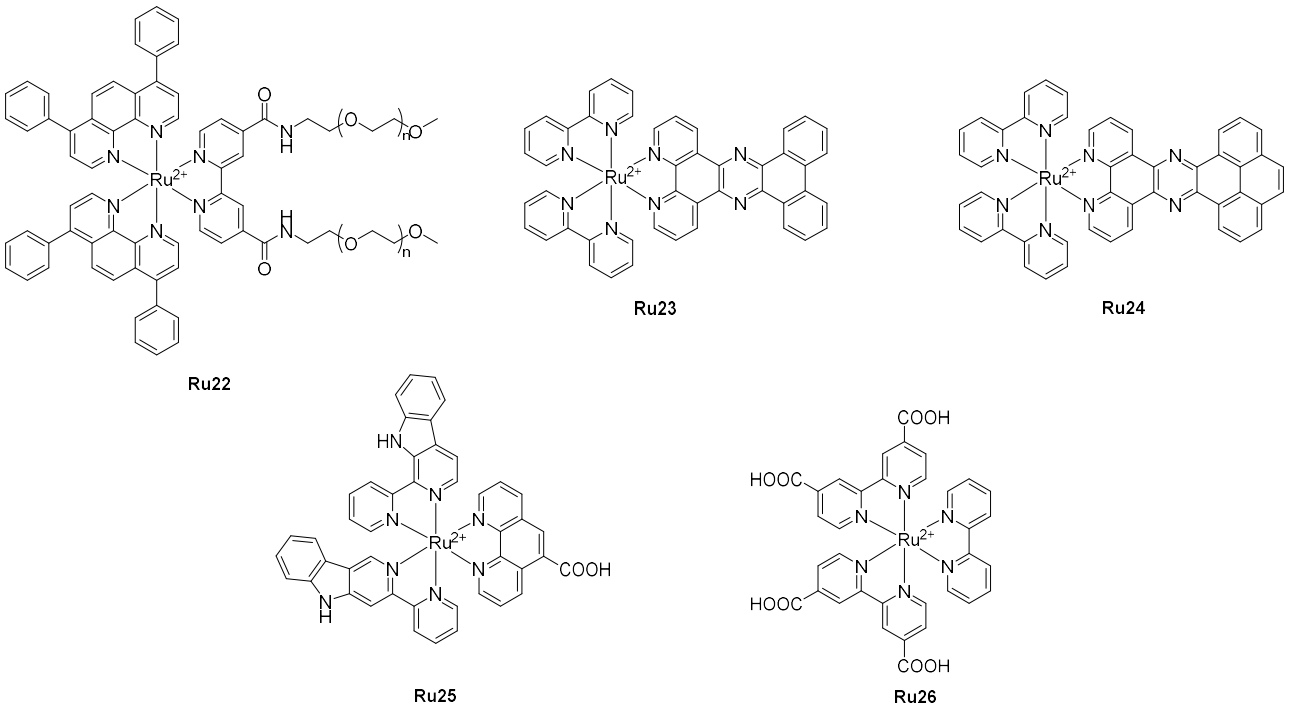

Figure 7. Chemical structures of **Ru22-Ru26.**

3.2. Porous nanomaterials

3.2.1. Porous silicon-based nanomaterials

Porous silicon-based nanoparticles refer to two types of nanomaterials: porous silicon nanoparticles (SiNPs) and mesoporous silica nanoparticles (MSNs).[62]

3.2.1.1. Porous silicon nanoparticles

SiNPs typically have a size around a few hundreds of nanometers or several microns. Their size, porosity, pore size, pore morphology, and surface chemistry can be tuned during the synthesis to achieve the optimal performance in drug delivery. However, these materials, which are inherently fluorescent, have only limited control on the three-dimensional porous structures distinguishing them from MSNs. Cunin, Lemercier and co-workers reported the multi-functionalization of SiNPs, including with the 2P Ru(II) luminescent complex $[Ru(5\text{-Fluo-Phen})_2(5\text{-E-Phen})]^{2+}$ (**Ru27**).[63] SiNPs were synthesized through electrochemical etching of silicon wafer, followed by sonication. They were then functionalized in a step-wise manner; the hydrosilylation of **Ru27** to the surface through the terminal alkyne moiety giving **SiNPs-Ru27** was followed by the silanization of surface hydroxyls with amine-terminated PEG to yield **SiNPs-Ru27-PEG** and finally the attachment of mannose (as cancer

targeting ligands) resulted in **SiNPs-Ru27-PEG-Man** with diameter ranging from 50 - 450 nm as characterized by TEM. The cytotoxicity of all the nanoparticles were evaluated against MCF-7 breast cancer cells and compared to that of the free complex: **SiNPs-Ru27** could reduce the cell viability down to 43 % with 1P excitation (420 – 440 nm, 14 J cm^{-2}, 20 min) and 36 % with 2P irradiation (800 nm, 3 scans of 1.57 s). Surprisingly, the incorporation of PEG and mannose did not improve significantly the 2P PDT efficacy.

3.2.1.2. Mesoporous silica nanoparticles

MSNs are solid materials with sizes ranging from 50 to 300 nm, containing hundreds of empty channels - called mesopores - in a 2D honeycomb-like network of porous structure. These nanoparticles possess a high surface area and pore volume, a stable meso-structure, a tunable pore diameter (*ca*. 2–10 nm), and facile surface modification (including the channels). This ordered pore network defines the size homogeneity, allowing a high loading capacity of drugs and enabling their controlled release. The loading of drugs into its matrix can be achieved by using different strategies: (i) entrapment by mixing the MSN precursors with the drug in a sol-gel phase before removing the liquid phase, (ii) encapsulation where the drug is loaded inside the pores as described for the entrapment strategy, followed by capping the pores, (iii) dissolution, (iv) adsorption relying on the attractive interaction between the silica surface and the drug molecules (physisorption) or (v) attachment taking advantage of the surface functionalization of MSNs by attaching drug molecules covalently on the surface (chemisorption), requiring a stimulus to cleave the covalent bond to release the drug.

Gómez-Ruiz, Gasser and co-workers reported the preparation of three Ru(II)-functionalized MSNs from the PDT PS **Ru7**: **MSN-CL-Ru7**, **MSN-CNO-Ru7** and **MSN-TRI-Ru7** with a diameter of around 77 nm.[64] They were prepared by functionalizing the surface of MSNs with two different silane coupling agents, 3-chloropropylethoxysilane and 3-isocyanatopropylethoxysilane, to give **MSN-CL** and **MSN-CNO**, respectively. The resulting materials reacted with the Ru complex to give **MSN-CL-Ru7** and **MSN-CNO-Ru7** with a Ru loading of 2.1 and 3.1 wt%, respectively. **MSN-CL** could also react with tri(2-aminoethyl)amine to give **MSN-TRI**, in which 7.5 wt% Ru complex was physically absorbed to give **MSN-TRI-Ru7**. Unfortunately, due to poor drug loading and quenching effect, these

nano-systems did not improve the photo-properties of the Ru(II) complex and were found to be not toxic towards HeLa cells.

Stoddart, Sauvage and Cryns developed a drug delivery platform obtained by grafting the surface of mesoporous silica nanoparticles with ruthenium(II) complexes.[65] A monodentate benzonitrile ligand was grafted onto the surface of MCM-41 (average nanopore diameter of 2 nm), followed by coordination of $[Ru(tpy)(dppz)(H_2O)]^{2+}$ (**Ru29**) under dark conditions at room temperature. Since the coordination between the Ru(II) complex and the monodentate ligand linked covalently to the nanoparticles can be cleaved under irradiation with visible light, **Ru29** can be released from the surface of the nanoparticles and can act as a potential anticancer agent. Moreover, other drugs such as the chemotherapeutic agent paclitaxel were loaded into MSNs pores for multi-modal therapy. In that case, the Ru(II) complex acted as a capping agent. Therefore, paclitaxel was first loaded into the pores and **Ru29** was then coordinated to block the pore openings. Light triggered first the release of **Ru29** before paclitaxel. The resulting nano-systems were toxic towards MDA-MB-468 breast cancer. The toxicity was mainly attributed to paclitaxel.

Chen and co-workers described the encapsulation of **Ru3** within *ca.* 100 nm arginine-glycine-aspartic acid (RGD) peptide-decorated MSNs.[66] The RGD peptide is the most used and effective tripeptide in targeting delivery because it can specifically bind to an integrin receptor, overexpressed in a wide range of tumor cells. The cytotoxicity of the resulting MSNs was evaluated in different cancer cells (*i.e.*, A375 melanoma, HepG2 hepatocellular carcinoma, MCF-7 breast adenocarcinoma, Neuro2a neuroblastoma and RHepG2 drug resistant carcinoma cells) and in HK-2 normal cells. The best results were obtained with A375 cells. Incorporation of RGD led to a significant enhancement in the uptake of the nanoparticles in A375 cells, which have the highest expression level of integrin receptors, *via* receptor-mediated endocytosis. This allowed a much higher anticancer effect with an IC_{50} of 65.8 nM while the IC_{50} value for **Ru3** was 5.9 μM and the unloaded RGD-functionalized MSNs showed no significant toxicity up to 400 μg mL^{-1}. It also improved the selectivity between cancer and healthy cells as the toxicity in HK-2 healthy cells were much lower with an IC_{50} higher than 75 μM. The release of **Ru3** from the nanoparticles were much faster in acidic conditions with 63.3 % of **Ru3** released at pH = 5.3 as opposed to 43.1 % at pH =

7.4. This is of interest since tumors are known to have an acidic environment. The cell death was attributed to apoptosis through ROS production.

3.2.2. Metal-organic frameworks

Metal-organic frameworks (MOFs) are organic–inorganic crystalline hybrid materials with permanent pores that are formed by the self-assembly of organic linkers and metal ions or clusters through coordination bonds. Like porous silicon-based nanoparticles and especially MSNs, MOFs have the advantages of high porosity, adjustable pore size, easy modification and good biocompatibility. Among the large family of MOFs, only zirconium-based MOFs have so far been used to incorporate Ru(II) polypyridyl complexes.

Lee and co-workers developed a zirconium-based MOF as a theranostic nanoplatform for combined two-photon imaging and PDT applications.[67] Ru(II) complexes have even been incorporated into MOF nanoparticles, with average diameters of 92 nm. Incorporation of $[Ru(bpy)_3]^{2+}$ (**Ru30**, Figure 8) into the pores of the MOFs resulted in an overall enhancement of the photophysical properties, including luminescence quantum yield, 2P absorption cross-section (σ_2 = 21.9 GM at 880 nm), $^1O_2$ generation and photostability compared to that of the free complex. Ru(II)–MOFs showed low toxicity towards HeLa cells in the dark at a concentration of 200 µg mL^{-1}. However, upon white light irradiation (200 mW cm^{-2}, 10 min), a significant reduction in the viability of the treated cells was observed.

Shi, Yao and co-workers reported a multifunctional MOF nanoplatform to combine PDT, PTT and chemotherapy.[68] Zirconium-based MOF, namely UiO-66, was functionalized with an azide group to perform a click reaction with a Ru(II) polypyridyl complex-based PDT PS bearing an alkyne group, **Ru31**, resulting in the formation of nanoparticles with a diameter of *ca.* 110 nm and a Ru loading of 10.2 %. The pores (1.64 nm) within these MOF nanoparticles acted as a host to 13.5 wt% of doxorubicin (DOX), and 6.8 wt% of copper sulfide (CuS) nanoparticles, a potential PTT agent, with a diameter of *ca.* 10 nm were loaded onto the surface of the nanoplatform by physical absorption. The structure of the framework was preserved throughout the chemical transformation. UiO-Ru27-DOX-CuS could generate $^1O_2$ efficiently upon excitation at 450 nm.

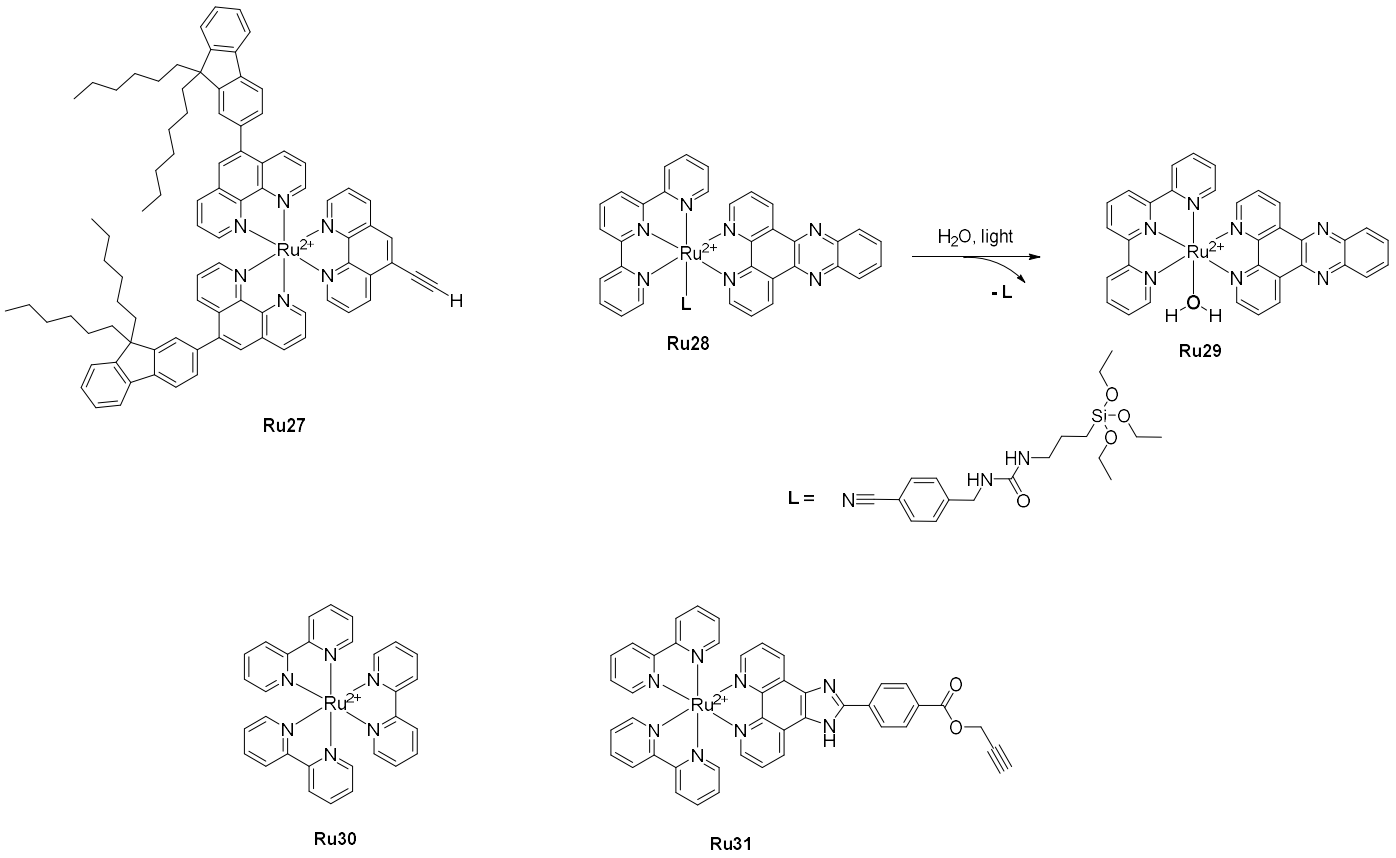

Figure 8. Chemical structures of **Ru27**-**Ru31**. Light-induced release of the monodentate ligand L leading to the formation of $[Ru(tpy)(dppz(H_2O)]^{2+}$ (**Ru29**).

3.3. Metal-based nanoparticles

3.3.1. Gold and silver nanoparticles

Gold and silver nanoparticles are very interesting nano-systems as they have intrinsic physical properties that could be used to construct a unique platform for potential multi-modal therapy. These nanoparticles are characterized by their surface plasmon resonance, which corresponds to a rise of plasmons when their surface is irradiated with an electromagnetic wave in the UV-visible region, leading to oscillation of conduction electrons. This feature can be used for detecting molecular interactions. For Ru(II) polypyridyl complexes, gold nanoparticles have so far been utilized to visualize and characterize biological processes at a molecular and cellular level.

Gunnlaugsson and co-workers reported the synthesis of three alkyl thiol group terminated Ru(II) polypyridyl complexes $[Ru(L)_2L']$$(PF_6)_2$ (L = bpy, phen or 1,4,5,8-tetraazaphenanthrene (TAB) and L' = 11-mercapto-N-(1,10-phenanthrolin-5-yl)undecanamide, **Ru32**, **Ru33**, **Ru34**) to react with surface-functionalized AuNPs (Figure 9).[69] The resulting sub-5 nm water-soluble AuNPs offered attractive

photophysical properties, ideal for applications in cellular imaging: they showed higher DNA affinity compared to the free Ru(II) complexes and no cytotoxicity towards HeLa cells after internalization and localization in the cytoplasm, allowing their potential use for cellular imaging. However, because of their small size, it was difficult to further investigate and characterize their uptake mechanism in cancer cells. The use of larger AuNPs of *ca.* 15-20 nm allowed visualization in cells using TEM.[70] They were observed within single membrane vesicles in the cytoplasm, suggesting a cellular uptake by endocytosis. Two of these Ru complexes, **Ru32** and **Ru33**, were also used by Shi and co-workers for functionalization of silver nanoparticles (AgNPs), resulting in monodisperse and homogeneous spherical nanoparticles with an average diameter of 20 nm.[71] AgNPs are known to induce cytotoxicity by an excessive generation of reactive oxygen species (ROS). Functionalization with Ru(II) complexes allowed cell imaging and enhanced anticancer activity. The Ru(II)-functionalized AgNPs were more toxic towards HeLa cells than the naked AgNPs, while the parent Ru complexes were not toxic up to 50 $\mu g \cdot mL^{-1}$. This improved cytotoxicity was attributed to an enhanced cellular uptake, hence an increase in ROS generation.

Pikramenou, Hodges and co-workers reported the functionalization of two Zonyl 7850 non-ionic fluorinated surfactant pre-coated AuNPs of different sizes (13 and 100 nm) with **Ru35**, a Ru(II) complex bearing two thiol groups and a hexyl spacer group to distance the Ru center from the nanoparticles' surface.[72] Pre-coating with a non-ionic fluorinated surfactant allowed a higher loading of Ru on the AuNPs surface by preventing irreversible aggregation. Attachment to AuNPs surface resulted in an enhancement in luminescence lifetime (from 260 ns for **Ru35** to 340 ns for **Ru35@AuNP13** and 360 ns for **Ru35@AuNP100**). Their strong luminescence allowed imaging in A549 cells with no significant cytotoxicity. The same authors then investigated the effect of the distance of the thiol-functionalized ruthenium luminescent center from the gold surface on the luminescence properties of the nanoparticles.[73] Three ruthenium probes with different length spacer units (**Ru35**, **Ru36** and **Ru37**) were attached on Zonyl pre-coated AuNPs of different sizes (13, 50 and 100 nm). An enhanced luminescence lifetime was obtained upon attachment with an increase of 20 %, 40 % and 70 % depending on the spacer length: the longer the spacer chain was, the higher the luminescence lifetime was. By contrast, AuNPs size did not affect it.

Chao and co-workers developed a strategy combining the 2P luminescence of Ru(II) polypyridyl complexes (**Ru38**, **Ru39** and **Ru40**, shown in Figure 9) and the photothermal properties of AuNPs in one single theranostic nanoplatform for image-guided PTT.[74] While the luminescence of Ru complexes was quenched upon attachment to AuNPs due to an energy transfer from the Ru(II) center to the AuNPs, the AuNPs still displayed significant 2P luminescence, which could be used in 2P lifetime imaging in cells, especially with **Ru39** (σ = 187 – 308 GM depending on the AuNPs size at 808 nm, 1 GM = 1 x 10-50 cm^4 s^{-1} $photon^{-1}$). The resulting AuNPs exhibited prominent photothermal conversion efficiency (18.3 % - 33.3% % as opposed to 7.3 % - 10.2 % for the naked AuNPs) and excellent photothermal stability. An effective tumor ablation was observed after photothermal treatment (808 nm, 0.8 W cm^{-2}, 5 min) *in vivo* on HeLa tumor-xenograft model mice.

As the best results were obtained with **Ru39**, they investigated the attachment of this Ru(II) complex on AuNPs with different morphologies: nanorods (AuNRs) with an average length of 40 ± 2.0 nm and width of 13 ± 0.8 nm and nanostars (AuNTs) with four tips of 15 – 25 nm long and a center sphere sizing 20 ± 1.3 nm.[75] The resulting **AuNRs@Ru37** and **AuNTs@Ru37** exhibited higher photothermal conversion efficient (η = 33.7 % for **AuNRs@Ru37**, η = 34.5 % for as opposed to η_{AuNRs} = 22.0%, η_{AuNTs} = 18.9%). Their cytotoxicity was evaluated in HeLa cells as well as in MCTSs and *in vivo* in a HeLa tumor-xenograft model. They showed similar results as of the ones obtained with AuNPs and good photothermal ablation at 808 nm using 0.25 $W{\cdot}cm^{-2}$ laser irradiation, which is lower than the maximal permissible exposure of skin by the American National Standard Institute (ANSI) regulation (0.33 $W{\cdot}cm^{-2}$ at 808 nm). The enhanced photothermal property was not dependent on the nanoparticle morphology.

Then they took advantage of the luminescence quenching effect of AuNPs to construct an off-on fluorescence probe for the detection of thiol-containing amino acids including glutathione (GSH), homocysteine (Hcy) and cysteine (Cys) in living cells.[76] AuNPs surface was modified with **Ru21** (shown in Figure 6) by reducing $HAuCl_4$ with $NaBH_4$ in the presence of the Ru(II) complex. Monodisperse and spherical Ru19@AuNPs, with diameters ranging from 4 to 11 nm, were obtained, in which the luminescence of the complex was completely quenched. Luminescence was restored when the nanoparticles reacted with thiol-containing compounds.

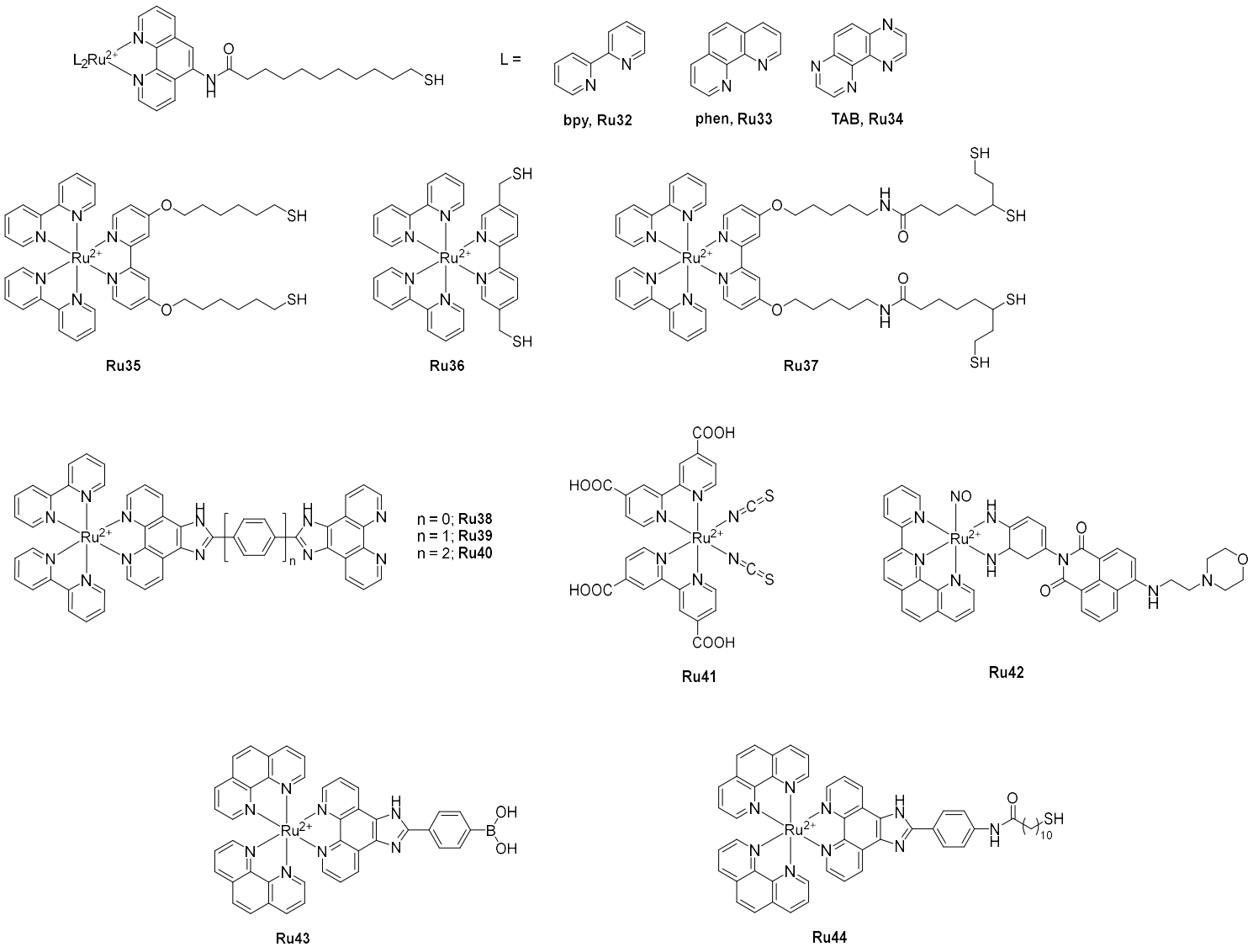

Figure 9. Chemical structures of Ru(II) polypyridyl complexes **Ru32 – Ru44** incorporated in metal-based and selenium nanoparticles.

3.3.2. Metal oxide nanoparticles

In addition to metal nanoparticles, which are predominantly gold and silver nanoparticles, metal oxide nanoparticles such as iron oxide (magnetite, Fe_3O_4) and titanium oxide (TiO_2) have also been investigated for cancer-related biomedical applications.

Sun, Zeng, and co-workers reported the preparation of fluorescent magnetic nanoparticles **Fe_3O_4-Ru** for simultaneous optical and magnetic resonance imaging applications.[77] $Ru(dcpy)_2(NCS)_2$ (**Ru41**) was coupled to Jeffamine-functionalized (M_n = 1900 g·mol^{-1}) magnetic Fe_3O_4 nanoparticles *via* the reaction of the amine end groups of Jeffamine with the isothiocyanate ligand of the Ru complex. Around 36 Ru complexes were incorporated onto the surface of each 8 nm Fe_3O_4

nanoparticle. Functionalization with Jeffamine not only afforded nanoparticles stable in biological media but also helped prevent the fluorescence quenching of the Ru complex by Fe_3O_4. **Fe_3O_4-Ru41** showed excellent colloidal, photochemical and magnetic stability. **Fe_3O_4-Ru41** nanoparticles were found in the cytoplasm of SK-BR-3 human breast cancer cells while showing no significant cytotoxicity.

Liu and co-workers developed a tumor-targeting system based on carbon-doped TiO_2 (C-TiO_2) nanoparticles for PACT applications.[78] Receptor-targeting folate molecules and 6.64 wt% of Ru(II) polypyridyl-nitrosyl complexes **Ru42**, bearing a lysosome-targeting morpholine moiety (Figure 9), were incorporated onto the surfaces of the 4 nm C-TiO_2 nanoparticles. The resulting nanoparticles exhibited excellent liposome specific colocalization in HeLa cells. NIR irradiation at 808 nm (600 mW cm^{-2}, 10 min) then led to the release of nitric oxide and ROS from the as prepared nanoparticles, resulting in a significant decrease in the viability of HeLa treated cells, with an $IC_{50light}$ value of 20 µg mL^{-1}. No significant toxicity was observed in the dark towards HeLa cells at the concentrations tested (10 – 200 µg mL^{-1}).

3.4. Selenium nanoparticles

Selenium, naturally present in trace amounts in the human body and required for the biosynthesis of selenocysteine-containing selenoproteins, has proven to be a potential anticancer agent in its nanoscale form. Decorating SeNPs with Ru(II) polypyridyl complexes could not only provide fluorescence for imaging but also an enhanced anticancer effect.

Tumor angiogenesis is the proliferation of a network of blood vessels, which provides the tumor with oxygen and nutrients required to grow. Blocking angiogenesis could be a strategy to inhibit and stop tumor growth. This strategy has been exploited by Liu and his research team. They reported the anti-angiogenesis and anti-tumor behavior of SeNPs decorated with $[Ru(phen)_2(p\text{-}BPIP)](PF_6)_2$ (**Ru43**, p-BPIP = (4-(1*H*-imidazo[4,5-*f*][1,10]phenanthrolin-2-yl)phenyl)boronic acid).[79] Fluorescent Ru-SeNPs were obtained, by reduction of Na_2SeO_3 with gallic acid prior to the addition of the Ru complex, as monodisperse homogeneous spherical particles with an average diameter of *ca*. 100 nm, characterized by TEM and an atomic ratio Se/Ru of 1/8. **Ru43-SeNPs**, compared to SeNPs or RuBP, could strongly inhibit at low concentrations (5 – 10 µg mL^{-1}) human umbilical vascular

endothelial cell (HUVEC) proliferation, migration, and tube formation, which are key steps for angiogenesis. The cytotoxicity of Ru39-SeNPs was examined against various cancerous cell lines and compared to that of the free Ru complex and naked SeNPs. **Ru43-SeNPs** showed a higher anti-tumor effect than the two counterparts: 4.8 ± 0.8 μg mL^{-1} for HUVEC, 3.1 ± 0.9 μg mL^{-1} for HepG2, 12.5 ± 1.2 μg mL^{-1} for SW480, 17.4 ± 1.5 μg mL^{-1} for PC-3 and 20.2 ± 2.3 μg mL^{-1} for MCF-7.

The same authors then described the functionalization of SeNPs with the thiol-based Ru(II) complex, $[Ru(phen)_2MUA](PF_6)_2$ (**Ru44**, MUA = 2-(4-11-mercaptoamide-*N*-phenyl)-1H-imidazo[4,5f][1,10]phenanthroline).[80] The resulting monodisperse and homogenous spherical nanoparticles of less than 100 nm, **Ru44@SeNPs**, enhanced the cellular uptake of **Ru44** in HepG2 cells with nuclear and cytoplasm localization, whereas **Ru44** was mainly localized in the cytoplasm. This resulted in significant cell damage at a relatively low concentration, IC_{50} = 18.5 μg mL^{-1}.

3.5. Upconversion nanoparticles

The biological application of Ru(II) polypyridyl complexes for PDT and PACT can somehow be limited by the need of the use of poorly penetrating blue or green light. Lanthanide-doped upconversion nanoparticles (UCNPs) can overcome this limitation as they can convert NIR photons to visible or UV light. Most reported UCNPs are hexagonal-phase $NaYF_4$ nanocrystals and the most common lanthanide ions used in photon upconversion are the pairs erbium(III)-ytterbium(III) or thulium(III)-ytterbium(III) (Figure 10).[81]

Salassa and co-workers were, to the best of our knowledge, the first to use UCNPs for the light-triggered release of photoactivated Ru(II) polypyridyl complexes with NIR irradiation. $[Ru(bpy)_2(py)_2]Cl_2$ (**Ru45**), where py is pyridine, was absorbed at the surface of UCNPs with a diameter of *ca.* 80 nm.[82] Irradiation at 980 nm could trigger photolysis to afford the aqua adduct $[Ru(bpy)_2(py)H_2O]Cl_2$. However, only one of the two monodentate ligands was able to dissociate from the complex, preventing potential interaction with DNA.

Liu and co-workers designed a drug delivery system using HSA coated UCNPs to efficiently deliver a photoactivated Ru(II) polypyridyl complex, **Ru4**.[83] The HSA coating made the particles highly biocompatible and well-dispersed in aqueous solution. HSA coated UCNPs were prepared by crosslinking HSA in the presence of UCNPs and **Ru4** using glutaraldehyde in ethanol/water solution.

Uniform spherical nanoparticle **Ru-HSA-UCNPs** with an average hydrodynamic diameter of 120 nm and a PDI of 0.092 were obtained. While the fluorescence was quenched after encapsulation of the Ru complex, HSA coating provided green fluorescence for cell imaging. **Ru-HSA-UCNPs** showed photo-induced cytotoxicity (white light, 10 min, 10 mW cm^{-2}) to HepG2 cells and HeLa cells attributed to the formation of $[Ru(bpy)_2(H_2O)_2]Cl_2$, which was shown to interact with DNA. No significant toxicity was observed in the dark (IC_{50} > 300 μM).

Wang and co-workers reported the encapsulation of a photoactivable Ru complex **Ru46** in UCNPs coated with PEG-modified lipid (DSPE-PEG, M_n = 5000 g mol^{-1}).[84] The resulting nanosystem had a core-shell structure with an average diameter of 670.4 nm. From the nanoparticles, 80 % of Ru complex was released as $[Ru(bpy)_2(H_2O)_2]_2$ after 2 h irradiation with visible light (λ > 400 nm, 0.07 W·cm^{-2}) or after 40 min irradiation with NIR light (980 nm, 3 W·cm^{-2}). The use of UCNPs could trigger the release of the DNA binding agent $[Ru(bpy)_2(H_2O)_2]^{2+}$ (**Ru47**) by NIR irradiation, suitable for deep-seated tumors, as shown in Figure 10b. However, no biological evaluation has been reported to date.

Due to the competing presence of a water absorption peak at the same wavelength requiring prolonged irradiation, the use of 980 nm light raises some concerns as it can deeply penetrate cells, therefore causing severe burns to biological systems. Bonnet and Natile described the conjugation of $[Ru(bpy)_2(\mathbf{3_H})](PF_6)_2$ (**Ru48**), a Ru(II) polypyridyl complex where $\mathbf{3_H}$ is a photocleavable bis(thioether) ligand modified with two phosphonate moieties, onto the surface of a core-shell-shell UCNPs (CSS-UCNPs) through its thioether groups.[85] They demonstrated that blue light could be generated from the resulting 115 nm particles after 796 nm irradiation at 50 W·cm^{-2}, allowing the photodissociation of the sulfur ligand from the Ru center. However, the photoreaction was not complete under therapeutically relevant conditions. Therefore, no biological evaluation was reported.

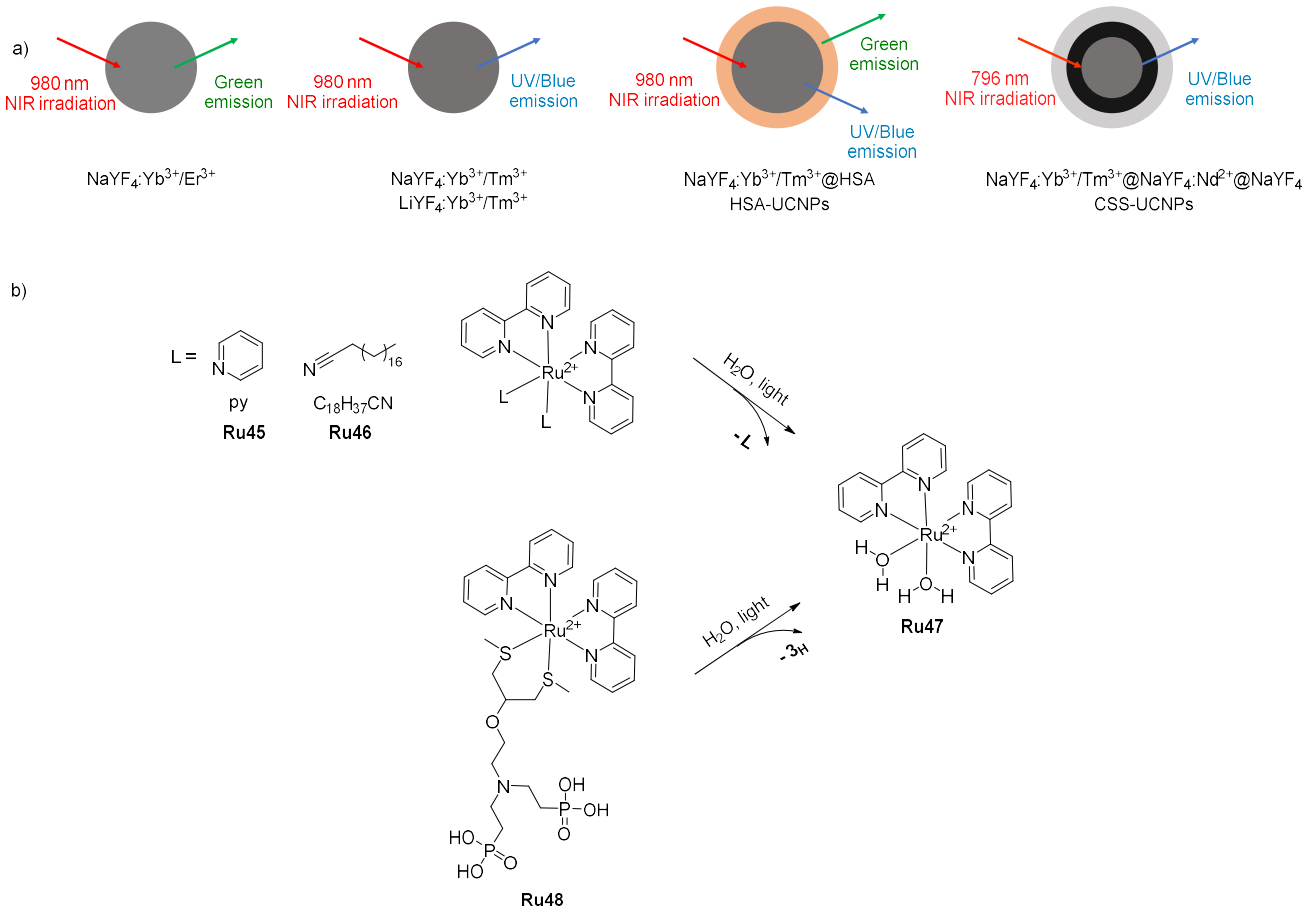

Figure 10. a) Schematic illustration of the various types of UCNPs used to incorporate photoactivatable Ru(II) polypyridyl complexes b) Photochemical activation of Ru(II) polypyridyl complexes where the monodentate ligand (L) or the bidentate ligand 3_H is photoexpelled from the Ru(II) complex upon irradiation with light.

Although very promising and innovative, upconversion nanoparticles, which can convert low-energy radiation to higher energy emissions enabling photo-induced therapy (*i.e.*, PDT and PACT) in deep tissues have more disadvantages than advantages.

4. Conclusions and Outlook

The use of Ru(II) polypyridyl complexes as biologically active agents for cancer therapy has been extensively investigated, especially since TLD1433 entered clinical trials. However, their low cellular uptake and cancer cells/tumors specificity have brought up the necessity to develop nanomaterials for the incorporation of Ru(II) polypyridyl complexes. Incorporation of Ru(II) polypyridyl complexes in nanoparticles is a promising strategy to design advanced nanomaterials with unique and attractive properties for biomedical applications. The development of Ru(II) polypyridyl complex-loaded nanomaterials is still in its infancy and much remains to be studied and understood. Depending on the intended application, an arsenal of nanoplatform constructs is available, ranging from organic to

inorganic materials, to incorporate Ru(II) polypyridyl complexes for cancer-related biomedical applications. While Ru(II) polypyridyl complexes have been encapsulated in polymeric and liposomal nanocarriers, they have mostly been incorporated onto the surface of inorganic nanomaterials. Organic nanocarriers are mainly used as transport vehicles for Ru(II) polypyridyl complexes, which protect them from biological and photo-degradation. As to inorganic nanoparticles, due to their inherent properties, they can provide multi-modal therapy, allowing for instance the coupling of PDT, PTT and imaging.

Based on the massive work already performed on the delivery of clinically approved drugs, including platinum-based complexes, the nano-systems currently in clinical trials are of the same nature and are mainly liposomal or, to a lesser extent polymeric, although multiple types of nanoparticles are available. The clinical trials of a few polymer-based nanocarriers for metal-based drugs (*e.g.*, NC-6004 Nanoplatin by NanoCarrier) have encouraged the development of the next generation of Ru(II) polypyridyl complexes. The incorporation of Ru(II) polypyridyl complexes into nanocarriers will offer exciting improvements in delivery, cell uptake and targeting for a more effective and safer therapy in the near future.

Biographies

Nancy Soliman received her MSc in Polymer Materials Science from the Université Pierre et Marie (now known as Sorbonne Université) in 2017. Interested in therapeutic and smart materials, she decided to undertake a PhD thesis with Prof. Christophe M. Thomas and Dr. Gilles Gasser (Chimie ParisTech, PSL University) on the design, synthesis, and characterization of well-defined biodegradable and biocompatible polymers for the delivery of biologically active Ru(II) polypyridyl complexes.

Gilles Gasser undertook a PhD thesis with Prof. Helen Stoeckli-Evans (University of Neuchâtel, Switzerland) and two post-docs, first with the late Prof. Leone Spiccia (Monash University, Australia) and then as an Alexander von Humboldt fellow with Prof. Nils Metzler-Nolte (Ruhr-University Bochum, Germany). In 2010, Gilles started his independent scientific career at the University of Zurich before moving, in 2016, to Chimie ParisTech, PSL University (Paris, France) to take a PSL Chair of Excellence.

Christophe M. Thomas obtained his PhD in Switzerland, working under the supervision of Prof. Süss-Fink. He then joined Prof. Coates' group at Cornell University (USA) as a post-doctoral fellow supported by the Swiss National Science Foundation. After spending one year in Prof. Ward's

laboratories, he was appointed as Assistant Professor at the University of Rennes (France) in 2004.

In 2008, he was promoted to Professor at Chimie ParisTech (PSL University, France).

References

[1] WHO / IARC Global cancer observatory Fact sheets http://gco.iarc.fr/today/data/factsheets/cancers/39-All-cancers-fact-sheet.pdf (accessed March 19, 2020).

[2] A. Juris, V. Balzani, F. Barigelletti, S. Campagna, P. Belser, A. Von Zelewsky, Coord. Chem. Rev. **1988**, *84*, 85.

[3] L. Tong, R. P. Thummel, *Chem. Sci.* **2016**, *7*, 6591.

[4] K. Kalyanasundaram, M. Grätzel, *Coord. Chem. Rev.* **1998**, *177*, 347.

[5] J. G. Vos, J. M. Kelly, *Dalton Trans.* **2006**, *0*, 4869.

[6] M. R. Gill, J. A. Thomas, *Chem. Soc. Rev.* **2012**, *41*, 3179.

[7] F. E. Poynton, S. A. Bright, S. Blasco, D. C. Williams, J. M. Kelly, T. Gunnlaugsson, *Chem. Soc. Rev.* **2017**, *46*, 7706.

[8] a) L. Zeng, P. Gupta, Y. Chen, E. Wang, L. Ji, H. Chao, Z.-S. Chen, *Chem. Soc. Rev.* **2017**, *46*, 5771; b) J. Liu, C. Zhang, T.W. Rees, L. Ke, L. Ji, H. Chao, *Coord. Chem. Rev.* **2018**, *363*, 17.

[9] A. Notaro, G. Gasser, *Chem. Soc. Rev.* **2017**, *46*, 7317.

[10] a) F. Heinemann, J. Karges, G. Gasser, *Acc. Chem. Res.* **2017**, *50*, 2727; b) M. Jakubaszek, B. Goud, S. Ferrari, G. Gasser, *Chem. Commun.* **2018**, *54*, 13040; c) P. S. Felder, S. Keller, G. Gasser, *Adv. Therap.* **2019**, 1900139

[11] J. D. Knoll, C. Turro, *Coord. Chem. Rev.* **2015**, *282–283*, 110.

[12] a) S. Monro, K. L. Colón, H. Yin, J. Roque, P. Konda, S. Gujar, R. P. Thummel, L. Lilge, C. G. Cameron, S. A. McFarland, *Chem. Rev.* **2019**, *119*, 797; b) Theralase Annouces First Patient Treated in Phase II Non-Muscle Invasive Bladder Cancer Clinical Study, https://www.streetinsider.com/dr/news.php?id=15879950&gfv=1, (accessed September 24, 2019); c) S. A. McFarland, A. Mandel, R. Dumoulin-White, G. Gasser, *Curr. Opin. Chem. Biol.* **2020**, *56*, 23.

[13] G. Chen, I. Roy, C. Yang, P. N. Prasad, *Chem. Rev.* **2016**, *116*, 2826.

[14] T. Sun, Y. S. Zhang, B. Pang, D. C. Hyun, M. Yang, Y. Xia, *Angew. Chem. Int. Ed.* **2014**, *53*, 12320.

[15] K. Cho, X. Wang, S. Nie, Z. Chen, D. M. Shin, *Clin. Cancer Res.* **2008**, *14*, 1310.

[16] U. Prabhakar, H. Maeda, K. R. Jain, M. E. Sevick-Muraca, W. Zamboni, C. O. Farokhzad, T. S. Barry, A. Gabizon, P. Grodzinski, C. D. Blakey, *Cancer Res.* **2013**, *73*, 2412.

[17] F. M. Veronese, A. Mero, *BioDrugs* **2008**, *22*, 315.

[18] R. Bazak, M. Houri, S. El Achy, S. Kamel, T. Refaat, *J. Cancer Res. Clin. Oncol.* **2015**, *141*, 769.

[19] F. Danhier, *J. Control. Release* **2016**, *244*, 108.

[20] S. Su, P.M. Kang, Nanomaterials **2020**,*10*, 656.

[21] a) M. Callari, J. R. Aldrich-Wright, P. L. de Souza, M. H. Stenzel, *Prog. Polym. Sci.* **2014**, *39*, 1614 ; b) E. Villemin, Y.C. Ong, C. M. Thomas, G. Gasser, *Nat. Rev. Chem.* **2019**, *3*, 261.

[22] T. C. Johnstone, K. Suntharalingam, S. J. Lippard, *Chem. Rev.* **2016**, *116*, 3436.

[23] V. Delplace, P. Couvreur, J. Nicolas, *Polym. Chem.* **2014**, *5*, 1529.

[24] a) E. Lepeltier, C. Bourgaux, P. Couvreur, *Adv. Drug Deliv. Rev.* **2014**, *71*, 86; b) C. J. Martínez Rivas, M. Tarhini, W. Badri, K. Miladi, H. Greige-Gerges, Q. A. Nazari, S. A. Galindo Rodríguez, R. Á. Román, H. Fessi, A. Elaissari, *Int. J. Pharm.* **2017**, *532*, 66.

[25] C. Vauthier, K. Bouchemal, *Pharm. Res.* **2009**, *26*, 1025; b) J. P. Rao, K. E. Geckeler, *Prog. Polym. Sci.* **2011**, *36*, 887.

[26] C. M. Thomas, J.-F. Lutz, *Angew. Chem. Int. Ed.* **2011**, *50*, 9244.

[27] G. Bœuf, G. V. Roullin, J. Moreau, L. Van Gulick, N. Zambrano Pineda, C. Terryn, D. Ploton, M. C. Andry, F. Chuburu, S. Dukic, M. Molinari, G. Lemercier, *ChemPlusChem* **2014**, *79*, 171.

[28] T. F. Chen, Y. A. Liu, W. J. Zheng, J. Liu, Y. S. Wong, *Inorg. Chem.* **2010**, *49*, 6366.

[29] L. Chan, Y. Huang, T. Chen, *J. Mater. Chem. B* **2016**, *4*, 4517.

[30] M. Dickerson, B. Howerton, Y. Bae, E. C. Glazer, *J. Mater. Chem. B* **2016**, *4*, 394.

[31] M. Appold, C. Mari, C. Lederle, J. Elbert, C. Schmidt, I. Ott, B. Stühn, G. Gasser, M. Gallei, *Polym. Chem.* **2017,** *8*, 890.

[32] A. Bordat, T. Boissenot, J. Nicolas, N. Tsapis, *Adv. Drug Deliv. Rev.* **2019**, *138*, 167.

[33] H. Ringsdorf, *J. Polym. Sci. Polym. Symp.* **1975**, *51*, 135.

[34] a) B. Happ, A. Winter, M. D. Hager, U. S. Schubert, *Chem. Soc. Rev.* **2012**, *41*, 2222–2255; b) V. Marin, E. Holder, R. Hoogenboom, U. S. Schubert, *Chem. Soc. Rev.* **2007**, *36*, 618; c) T. Mede, M. Jäger, U. S. Schubert, *Chem. Soc. Rev.* **2018**, *47*, 7577.

[35] D. Maggioni, F. Fenili, L. D'Alfonso, D. Donghi, M. Panigati, I. Zanoni, R. Marzi, A. Manfredi, P. Ferruti, G. D'Alfonso, E. Ranucci, *Inorg. Chem.* **2012**, *51*, 12776.

[36] L. Mascheroni, M. V. Dozzi, E. Ranucci, P. Ferruti, V. Francia, A. Salvati, D. Maggioni, *Inorg. Chem.* **2019**, *58*, 14586.

[37] W. Sun, M. Parowatkin, W. Steffen, H.-J. Butt, V. Mailänder, S. Wu, *Adv. Healthcare Mater.* **2016**, *5*, 467.

[38] W. Sun, Y. Wen, R. Thiramanas, M. Chen, J. Han, N. Gong, M. Wagner, S. Jiang, M. S. Meijer, S. Bonnet, H.-J. Butt, V. Mailänder, X.-J. Liang, S. Wu, *Funct. Mater.* **2018**, *28*, 1804227.

[39] W. Sun, S. Li, B. Häupler J. Liu, S. Jin, W. Steffen, U. S. Schubert, H.-J. Butt, X.-J. Liang, S. Wu, *Adv. Mater.* **2016**, *29*, 1603702.

[40] H. R. Kricheldorf and I. Kreiser-Saunders, *Polymer* **1994**, 35, 4175.

[41] J. Nicolas, *Chem. Mater.* **2016**, 28, 1591.

[42] N. Soliman, L. K. McKenzie, J. Karges, E. Bertrand, M. Tharaud, M. Jakubaszek, V. Guérineau, B. Goud, M. Hollenstein, G. Gasser, C. M. Thomas, *Chem. Sci.* **2020**, *11*, 2657.

[43] P. Kesharwani, K. Jain, N. K. Jain, *Prog. Polym. Sci.* **2014**, *39*, 268.

[44] A. Ruggi, C. Beekman, D. Wasserberg, V. Subramaniam, D. N. Reinhoudt, F. W. B. van Leeuwen, A. H. Velders, *Chem.: Eur. J.* **2011**, *17*, 464.

[45] T. M. Allen, P. R. Cullis, *Adv. Drug Deliv. Rev.* **2013**, *65*, 36.

[46] J. Shen, H.-C. Kim, J. Wolfram, C. Mu, W. Zhang, H. Liu, Y. Xie, J. Mai, H. Zhang, Z. Li, M. Guevara, Z.-W. Mao, H. Shen, *Nano Lett.* **2017**, *17*, 2913.

[47] L.-L. Huang, J. Xu, Y.-J. Jin, D.-X. Zhao, H.-Y. Xie, *Analyst*, **2016**, *141*, 2948.

[48] S. Bonnet, B. Limburg, J. D. Meeldijk, R. J. M. Klein Gebbink, J. A. Killian, *J. Am. Chem. Soc.* **2011**, *133*, 252.

[49] S. H. C. Askes, A. Bahreman, S. Bonnet, *Angew. Chem. Int. Ed.* **2014**, *53*, 1029.

[50] S. H. C. Askes, M. Kloz, G. Bruylants, J. T. Kennis, S. Bonnet, *Phys. Chem. Chem. Phys.* **2015**, *17*, 27380.

[51] D. Desmaële, R. Gref, P. Couvreur, *J. Control. Release* **2012**, *161*, 609.

[52] M. Ceruti, G. Balliano, F. Viola, *Eur. J. Med. Chem.* **1987**, *22*, 199.

[53] F. Dosio, B. Stella, A. Ferrero, C. Garino, D. Zonari, S. Arpicco, L. Cattel, S. Giordano, R. Gobetto, R. *Int. J. Pharm.* **2013**, *440*, 221.

[54] S. Chakrabortty, B. K. Agrawalla, A. Stumper, N. M. Vegi, S. Fischer, C. Reichardt, M. Kögler, B. Dietzek, M. Feuring-Buske, C. Buske, S. Rau, T. Weil, *J. Am. Chem. Soc.* **2017**, *139*, 2512.

[55] J. Liu, L. Cui, D. Losic, *Acta Biomater.* **2013**, *9*, 9243.

[56] D.-Y. Zhang, Y. Zheng, C.-P. Tan, J.-H. Sun, W. Zhang, L.-N. Ji, Z.-W. Mao, *ACS Appl. Mater. Interfaces* **2017**, *9*, 6761.

[57] a) A. Bianco, K. Kostarelos, M. Prato, *Curr. Opin. Chem. Biol.* **2005**, *9*, 674; b) N. Kobayashi, H. Izumi, Y. Morimoto, *J. Occup. Health* **2017**, *59*, 394.

[58] P. Zhang, H. Huang, J. Huang, H. Chen, J. Wang, K. Qiu, D. Zhao, L. Ji, H. Chao, *ACS Appl. Mater.* Interfaces **2015**, *7*, 23278.

[59] N. Wang, Y. Feng, L. Zeng, Z. Zhao, T. Chen, *ACS Appl. Mater. Interfaces* **2015**, *7*, 14933.

[60] D.-Y. Zhang, Y. Zheng, H. Zhang, L. He, C.-P. Tan, J.-H. Sun, W. Zhang, X. Peng, Q. Zhan, L.-N. Ji, Z.-W. Mao, *Nanoscale* **2017**, *9*, 18966.

[61] D. Yang, S. Guan, Y. Niu, Z. Xie, S. Zhou, X. Qu, *J. Mater. Chem. B* **2018**, *6*, 2315.

[62] Y. Yu, X. Liu, in *Nanobiomaterials*, (Eds: X. Wang, M. Ramalingam, X. Kong, L. Zhao), John Wiley & Sons, Ltd, **2017**, pp. 379.

[63] N. Ž. Knežević, V. Stojanovic, A. Chaix, E. Bouffard, K. E. Cheikh, A. Morère, M. Maynadier, G. Lemercier, M. Garcia, M. Gary-Bobo, J.-O. Durand, F. Cunin, *J. Mater. Chem. B* **2016**, *4*, 1337.

[64] Y. Ellahioui, M. Patra, C. Mari, R. Kaabi, J. Karges, G. Gasser, S. Gómez-Ruiz, *Dalton Trans.* **2019**, *48*, 5940.

[65] M. Frasconi, Z. Liu, J. Lei, Y. Wu, E. Strekalova, D. Malin, M. W. Ambrogio, X. Chen, Y. Y. Botros, V. L. Cryns, J.-P. Sauvage, J. F. Stoddart, *J. Am. Chem. Soc.* **2013**, *135*, 11603.

[66] L. He, Y. Huang, H. Zhu, G. Pang, W. Zheng, Y.-S. Wong, T. Chen, *Adv. Funct. Mater.* **2014**, *24*, 2754.

[67] R. Chen, J. Zhang, J. Chelora, Y. Xiong, S. V. Kershaw, K. F. Li, P.-K. Lo, K. W. Cheah, A. L. Rogach, J. A. Zapien, C.-S. Lee, *ACS Appl. Mater. Interfaces* **2017**, *9*, 5699.

[68] X. Hu, Y. Lu, C. Dong, W. Zhao, X. Wu, L. Zhou, L. Chen, T. Yao, S. Shi, Chem. Eur. J. **2020**, *26*, 1668.

[69] R. B. P. Elmes, K. N. Orange, S. M. Cloonan, D. C. Williams, T. Gunnlaugsson, *J. Am. Chem. Soc.* **2011**, *133*, 15862.

[70] M. Martínez-Calvo, K. N. Orange, R. B. P. Elmes, B. la Cour Poulsen, D. C. Williams, T. Gunnlaugsson, *Nanoscale* **2016**, *8*, 563.

[71] M. Wumaier, T.-M. Yao, X.-C. Hu, Z.-A. Hu, S. Shi, *Dalton Trans.* **2019**, *48*, 10393.

[72] N. J. Rogers, S. Claire, R. M. Harris, S. Farabi, G. Zikeli, I. B. Styles, N. J. Hodges, Z. Pikramenou, *Chem. Commun.* **2014**, *50*, 617.

[73] S. A. M. Osborne, Z. Pikramenou, *Faraday Discuss.* **2015**, *185*, 219.

[74] P. Zhang, J. Wang, H. Huang, B. Yu, K. Qiu, J. Huang, S. Wang, L. Jiang, G. Gasser, L. Ji, H. Chao, *Biomaterials* **2015**, *63*, 102.

[75] P. Zhang, J. Wang, H. Huang, K. Qiu, J. Huang, L. Ji, H. Chao, *J. Mater. Chem. B* **2017**, *5*, 671.

[76] P. Zhang, J. Wang, H. Huang, H. Chen, R. Guan, Y. Chen, L. Ji, H. Chao, *Biomaterials* **2014**, *35*, 9003.

[77] P. Xi, K. Cheng, X. Sun, Z. Zeng, S. Sun, *J. Mater. Chem.* **2011**, *21*, 11464.

[78] H.-J. Xiang, Q. Deng, L. An, M. Guo, S.-P. Yang, J.-G. Liu, J.-G. *Chem. Commun.* **2016**, *52*, 148.

[79] D. Sun, Y. Liu, Q. Yu, Y. Zhou, R. Zhang, X. Chen, A. Hong, J. Liu, *Biomaterials* **2013**, *34*, 171.

[80] D. Sun, Y. Liu, Q. Yu, X. Qin, L. Yang, Y. Zhou, L. Chen, J. Liu, *Biomaterials* **2014**, *35*, 1572.

[81] a) E. Ruggiero, S. A. Castro, A. Habtemariam, L. Salassa, *Dalton Trans.* **2016**, *45*, 13012; b) S. Wu, H.-J. Butt, *Adv. Mater.* **2016**, *28*, 1208.

[82] E. Ruggiero, A; Habtemariam, L. Yate, J. C. Mareque-Rivas, L. Salassa, *Chem. Commun.* **2014**, *50*, 1715.

[83] H. Shi, T. Fang, Y. Tian, H. Huang, Y. Liu, *J. Mater. Chem. B* **2016**, *4*, 4746.

[84] Y. Chen, G. Jiang, Q. Zhou, Y. Zhang, K. Li, Y. Zheng, B. Zhang, X. Wang, *RSC Adv.* **2016**, *6*, 23804.

[85] S. M. Meijer, M. M. Natile, S. Bonnet, *Inorg. Chem.* **2020**, https://doi.org/10.1021/acs.inorgchem.0c00043.